Supplementary Information for:

Discovery and characterization of UipA, a uranium- and iron-binding PepSY protein involved in uranium tolerance by soil bacteria.

Nicolas Gallois, Béatrice Alpha-Bazin, Philippe Ortet, Mohamed Barakat, Nicolas Bremond, Laurie Piette, Nicolas Theodorakopoulos, Abbas Mohamad Ali, David Lemaire, Pierre Legrand, Magali Floriani, Laureline Février, Christophe den Auwer, Pascal Arnoux, Catherine Berthomieu, Jean Armengaud, Virginie Chapon

Correspondence to: Virginie Chapon

virginie.chapon@cea.fr

This pdf includes:

Detailed Methods and References

Figs. S1-S39

Tables S5 and S8

Detailed Methods:

Uranium tolerance of *Microbacterium*: drop test assay

Bacteria were cultured in LB at 32°C with shaking until the exponential growth phase, and were then exposed to uranyl following the same procedure as described in [1]. Briefly, cells were suspended in 0.1 M NaCl (pH 5.0) with 0, 10, 50, 100, 250, or 500 µM U(VI) (prepared with a stock solution of uranyl nitrate at 50 mM in 2% HCl) and incubated 24 h at 25°C. After uranium exposure, cells were washed twice with 0.1 M NaCl (pH 5.0) and resuspended at approximately $6x10^9$ cells mL^{-1} in 0.1 M NaCl (pH 5.0). Finally, 20-µL drops of each cell suspension were deposited on LB agar and incubated for 48 h at 32°C to estimate cell survival.

Interactions of *Microbacterium* sp. strains with uranyl

The experimental procedure is described in detail in [1]. Bacteria were cultured in LB at 32°C with shaking until the exponential growth phase, and were then washed with 0.1 M NaCl (pH 5.0). The cell pellet was resuspended in 0.1 M NaCl (pH 5.0) with 0 or 10 µM U(VI) at a final $OD_{600\ nm}$ = 1 and incubated at 25°C with shaking. Fractions of 1 mL of cell suspension were taken after 0.5, 2, 4, 6, 10, and 24 h exposure. Samples were centrifuged for 5 min at 8000 g, and uranium concentration was measured in the supernatant by inductively coupled plasma-atomic emission spectrometry (ICP-AES Optima 4300DV, PerkinElmer). Controls without bacteria demonstrated that uranium remains

soluble and that no loss of uranium due to adsorption on the vial wall occurred within the 24h exposure experiment. Cell pellets were immediately frozen in liquid nitrogen and kept at -80°C until the proteomic analysis. Four independent biological replicates were made. Blank controls without bacteria were performed. The fraction of uranium associated with the cells was calculated as follows: $U_{cells} = (U_{blank} – U_{solution})*100/U_{blank}$. Ultra-thin sections of bacterial cells exposed to uranium for 24 h were analyzed by transmission electron microscopy.

Shotgun proteomic analysis

Samples for the proteomic analysis were prepared as described in [2]. Briefly, cell pellets were lysed by sonication and subjected to a short migration on SDS-PAGE in denaturing conditions. The whole proteome content (comprising soluble and membrane proteins) was excised from the gel and submitted to in-gel proteolysis with trypsin. NanoLC-MS/MS experiments were performed using a Q-Exactive HF mass spectrometer (ThermoFisher) coupled to an UltiMate 3000 LC system (Dionex-LCPackings). Peptide mixtures were loaded on a reverse phase precolumn and desalted on-line. Peptides were resolved onto a reverse phase Acclaim PepMap 100 C18 column and injected into the QExactive HF mass spectrometer. The Q-Exactive HF instrument was operated according to a Top20 data-dependent acquisition method, as described previously in [3].

Bioinformatics analysis was conducted as described in [2], with the exception of the use of an in-house protein sequence database derived from the complete genomes of the *Microbacterium* strains[4]. Briefly, the recorded MS/MS spectra were searched against the in-house protein database using the MASCOT engine. All peptide matches with a peptide score above its query threshold set at $p \leq 0.05$ and rank 1 were parsed using the IRMa 1.31.1c software [5]. MS/MS spectra assigned to several loci were systematically removed. A protein was considered validated when at least two different peptides were detected. The number of MS/MS spectra per protein (spectral counts) was determined for the four replicates from each of the three time points for every condition. The protein abundances were compared for each time point between the uranyl exposure and the control condition. For each of these comparisons, a list of non-redundant proteins detected among the six corresponding datasets was established. The total spectral count of each polypeptide was used to rank the proteins from highest to lowest detection intensity. The statistical protein variation among the four replicate samples for the two compared specific exposure conditions was calculated using the T-Fold option in the PatternLab 2.0 software [6]. This module makes it possible to normalize the spectral count datasets, calculate the average fold changes with statistics (t-test), and estimate the resulting theoretical false discovery rate. Normalization was conducted by taking into account the total number of spectral counts for each sample, with at least two readings per protein. A minimum value of 1 was systematically added to all spectral count values in order to consider missing

values as a standard PatternLab normalization. Parameters for the comparisons were as follows: minimum fold-change of 1.5, minimum p-value of 0.05, and BH-FDR Alfa of 0.15. Normalized spectral abundance factor (NSAF) for each protein was calculated using the formula: (spectral counts / theoretical molecular weight) × 1000, as previously proposed [7]. The mass spectrometry proteomics data were deposited in a public repository at the ProteomeXchange Consortium (http://proteomecentral.proteomexchange.org) via the PRIDE partner repository [8], with the dataset identifiers: PXD020778 and 10.6019/PXD020778 for *Microbacterium* sp. HG3; PXD020767 and 10.6019/PXD020767 for *Microbacterium lemovicicum* Viu22; PXD020737 and 10.6019/PXD020737 for *Microbacterium* sp. Viu2A; and PXD020998 and 10.6019/PXD020998 for *Microbacterium oleivorans* sp. A9.

Topology of UipA

To determine the *in vivo* orientation of the UipA membrane protein, the pKtop plasmid encoding a dual phoA-LacZα reporter was used [9]. Three pKtop derivatives were constructed in which *phoA-lac* was fused in frame after the *uipA-ViU2A* codons R70, G96 and D281. The constructions were made by overlap extension PCR cloning according to the methods of [10]. In a first PCR, the inserts were amplified with the primer UipA_pKtop_F: **ATTACGCCAAGCTTGCATGCC**GACGACAAGACACCCACCCC and one of the following primers: UipA_R69-pKtop-R: **ATCCTCTAGAGTCGACCTGCA**GCGCGTGCGGCCGGGCTT; UipA_G96-pKtop-R: **ATCCTCTAGAGTCGACCTGC**AGCCGATCGCCGCGCCGAC; or UipA_D281-pKtop-R: ATCCTCTAGAGTCGACCTGCAGTCGATGTCGGTTCCGACG. The sequences in bold correspond to regions of overlap with the pKtop plasmid. PCR amplifications were performed using Phusion Flash Master Mix (ThermoFisher Scientific) and ViU2A cell suspensions under the following conditions: 5 min at 98°C; followed by 30 cycles of 10 sec at 98°C, 10 sec at 58°C and 15 sec at 72°C; and a final step of 15 sec at 72°C. PCR products were purified and used as megaprimers to perform a second PCR using Phusion Flash Master Mix (ThermoFisher Scientific) and 50 ng of purified pKtop under the following conditions: 30 sec at 98°C; followed by 25 cycles of 30 sec at 98°C, 30 sec at 55°C and 5 min at 72°C; and a final step of 5 min at 72°C. PCR products were digested by *DpnI* to eliminate the original plasmid templates, and were transformed in *E.coli*. Transformants were selected on LB agar plates containing 50 µg/mL kanamycin and 0.2% glucose incubated for 26 h at 30°C. For *in vivo* protein topology assays, freshly transformed colonies were streaked on dual indicator LB agar plates supplemented with kanamycin (50 µg/mL), IPTG (1 mM), 6-chloro-3-indolyl-β-D-galactoside (Red-Gal; 100 µg/mL); and disodium 5-bromo-4-chloro-3-indolyl phosphate (BCIP; 80 µg/mL). Plates were incubated for 24 h at 30°C, and 14 h at room temperature.

Production and purification of the extracellular domain of UipA proteins

DNA fragments coding for the soluble domain of UipA proteins (UipA-out) were amplified with specific primer sets as follows:

- for $UipA_{A9}$-out:

UipA_A9_BamHI-TEV_F_pQE: GAGAGGATCC**GAGAACCTGTACTTCCAGTCC**CTGGCGGACGACCGCG;
UipA_A9_HindIII_R_pQE: GAGAAAGCTTTCAGTCGTCGAGTTCGGTCGCCAGGACCTTCCC

- for $UipA_{ViU2A}$-out and $UipA_{HG3}$-out:

UipA_Hg3_BamHI-TEV_F_pQE GAGAGGATCC**GAGAACCTGTACTTCCAGTCC**ATCGGCGACGAGTTCG;
UipA_Hg3_HindIII_R_pQE GAGAAAGCTTTCAGTCGATGTCGGTACCGACGACCGCGAAGTCGGCG.

These primer sets introduce a *BamHI* restriction site and a TEV protease recognition site (in bold) upstream of the start codon, and a *HindIII* restriction site after the last codon. PCR amplification was performed using 1 U Taq polymerase (Prime Star; Lonza) and 200 ng of purified genomic DNA under the following conditions: 2 min at 95°C; followed by 25 cycles of 30 sec at 95°C, 30 sec at 60°C, and 1 min at 72°C; and a final elongation at 72°C for 5 minutes. After digestion with *BamHI* and *HindIII* enzymes, the DNA fragments were purified and ligated into the *BamHI* and *HindIII* sites of the pQE30 plasmid to obtain pQE-UipA recombinant plasmids for each of the three homologs. The recombinant plasmids were transformed in *E. coli* XL1 Blue (Stratagene) and verified by sequencing. Each version of the pQE-UipA plasmid was then transformed in *E. coli* M15Rep4 (Qiagen). Transformants were cultured at 37°C in LB medium containing ampicillin (50 $\mu g.mL^{-1}$) and kanamycin (50 $\mu g.mL^{-1}$) until the exponential growth phase (OD_{600nm} = 0.5), and expression of the recombinant proteins was induced by addition of 0.1 mM isopropyl-D-thiogalactoside. The cultures were then incubated overnight at 17°C. Cells were lysed with a One Shot Cell Disrupter (Constant Systems Limited) and centrifuged for 30 min at 15,000 rpm to remove cell debris. The supernatant was then loaded at a flow rate of 1 $mL.min^{-1}$ on a 5-mL HiTrap HP chelation column (GE Healthcare) in buffer A (50 mM Tris-HCl, 0.5 M NaCl, 25 mM imidazole buffer pH 7.5) containing 1 mM AEBSF. The recombinant proteins were eluted from the resin at a flow rate of 1 $mL.min^{-1}$ with three successive steps of 9:1, 1:1 and 0:1 ratio of buffer A / buffer B (50 mM Tris-HCl, 0.5 M NaCl, 500 mM imidazole buffer pH 7.5). The fractions eluted during the first two steps and containing the protein of interest were pooled, desalted on a HiPrep 26/10 desalting column (GE Healthcare), and incubated 48 h at 4°C under gentle agitation with TEV protease to cut the His tags. The samples were loaded on a HiTrap HP column, and the recombinant proteins without the His tag were collected in the eluate fraction. A final step of purification was performed on an exclusion chromatography column (HiLoad Superdex 75, Healthcare) in 50 mM Tris-HCl, 100 mM NaCl (pH 7.5) to increase the purity. Protein concentration was measured using the BCA (Uptima) assay with standard bovine serum albumin. Protein purity and

integrity were checked by SDS-PAGE and mass spectrometry (MS) in denaturing conditions (MicrOTOF-Q Bruker with an electrospray ionization source). For MS, sample concentration was 1 µM in CH_3CN/H_2O (1/1-v/v), 0.2% formic acid (Sigma-Aldrich). Samples were continuously infused at a flow rate of 3 µl.min^{-1}. Mass spectra were recorded in the 50-7000 mass-to-charge (m/z) range. MS experiments were carried out with a capillary voltage set at 4.5 kV and an end plate off set voltage of 500 V. The gas nebulizer (N_2) pressure was set at 0.4 bars and the dry gas flow (N_2) at 4 L.min^{-1} and a temperature of 190°C.

Non-covalent mass spectrometry

Mass spectrometry analyses were performed on a MicrOTOF-Q (Bruker, Wissembourg, France) with an electrospray ionization source. Protein-metal complexes were prepared by mixing UipA proteins at 10 µM in 20 mM ammonium acetate (Sigma-Aldrich) with 5 µM uranyl. For $UipA_{ViU2A}$, 100 µM IDA was added to the mixture. However, its absence did not modify the result (data not shown), so it was omitted for $UipA_{HG3}$ and $UipA_{A9}$. The samples were continuously infused at a flow rate of 7 µL.min^{-1}. The mass spectra were recorded in the 50-4000 mass-to-charge (*m/z*) range. The gas nebulizer (N_2) pressure was set at 3 bars and the dry gas flow (N_2) at 3/min and a temperature of 200°C. Data were acquired in the positive mode and calibration was performed using a calibrating solution of ESI Tune Mix (Agilent) in CH_3CN/H_2O (95/5-v/v). The system was controlled using the MicrOTOF Control 2.2 software package, and data were processed with DataAnalysis 3.4.

Metal-binding affinities of the UipA soluble domain measured by fluorescence titration

The metal binding affinities of the three UipA-out peptides for different metal cations (UO_2^{2+}, Fe^{3+}, Cu^{2+}, Ca^{2+}, Ni^{2+} and Zn^{2+}) were examined by monitoring the fluorescence intensity of tryptophan ($UipA_{ext}$-A9: Trp144) or tryptophan and tyrosine ($UipA_{ext}$-HG3: Trp183, Tyr257 and $UipA_{ext}$-ViU2A: Trp179 and Tyr253). To remove all traces of metal from the samples prior to the fluorimetry experiments, each protein solution was incubated for 2 h with 3 mM EDTA. The proteins were then washed 10 times through 3 kDa Amicon Ultra centrifugal filters (Merk Millipore, Watford, UK). The uranyl and iron solutions were prepared extemporaneously by diluting a 50 mM stock solution of uranyl nitrate (in 2% HCl, pH 3.5, kept frozen at -20°C) and a 50 mM stock solution of iron chloride (in 2% HCl, prepared extemporaneously) in ultrapure water to a final concentration of 1.25 mM. For fluorescence titrations in the presence of uranyl or iron, iminodiacetate (IDA) was added to the peptide solution at an IDA/peptide ratio of 10:1 (typically 100 µM), in order to avoid the formation of hydroxo complexes and to control iron and uranyl speciation. The experiments were carried out with 10 µM protein in 20 mM MES buffer 100 mM KCl pH 6. Fluorescence was measured on a Cary Eclipse fluorescence spectrometer (Agilent Technologies, CA, USA) at 25°C using a 275-nm excitation

wavelength. Emission was recorded from 300 to 380 nm. The excitation and emission slits were 10 nm. The reported dissociation constants are averages of three experimental values including standard deviation.

Competition experiments between the UipA-out proteins and IDA were performed to determine the conditional dissociation constants of the protein-cation complexes (uranyl or iron) at pH 6. IDA binds uranyl and iron with moderate affinity and forms three and two complexes, respectively: UO_2IDA, $[UO_2(IDA)_2]^{2-}$, $[(UO_2)_2(IDA)_2(OH)_2]^{2-}$ and $[FeIDA]^+$, $[Fe(IDA)_2]^-$. The conditional stability constants of the three uranyl-IDA species were calculated from the stability constants at 25°C and 0.1 M ionic strength provided in [11]. For iron-IDA complexes, stability constants were obtained from [12]. All conditional stability constants were fixed in the analysis of the spectral data, which was performed using the ReactLab software [13].

Fourier-transformed infrared spectroscopy

For Fourier-transformed infrared spectroscopy (FTIR), proteins were concentrated to approximately 500 µM with 3 kDa Amicon Ultra centrifugal filters (Merck Millipore, Watford, UK) in 20 mM MES buffer (pH 6). Uranyl or iron from stock solutions of uranyl nitrate and iron chloride at 50 mM in 2% HCl were added to reach a stoichiometric peptide:metal ratio of 1:1. In parallel, control samples were prepared in 20 mM MES buffer (pH 6) by adding an equivalent volume of 2% HCl solution. The samples with proteins were then immediately deposited onto the ATR-FTIR crystal. Spectra were acquired 0, 120, 1020 and 1920 seconds after deposition. Comparison between the last two spectra (taken at 1020 s and 1920 s) ensured that the sample was completely dry on the crystal. This was necessary in order to obtain reliable difference spectra between samples with or without metal cations. The crystal was thoroughly washed with ultrapure water and a 50:50 water/ethanol mixture, and was dried between two consecutive measurements. The spectra were recorded on an IFS66 SX FTIR spectrometer (Bruker) equipped with a KBr beam splitter, a DTGS-KBR detector, and an attenuated total reflection device (ATR) (SensIR Technologies, CT) equipped with a 4.3-mm diameter diamond 9-bounce microprism and ZnSe optics. Each single spectrum corresponded to 50 co-added scans at a resolution of 4 cm^{-1}. All reported frequencies have an accuracy of ± 1 cm^{-1}. The spectra correspond to the average of data recorded with 2 to 4 replicates in the same conditions. To calculate the difference spectra between uranyl or iron-containing samples and control samples, interactive subtraction was used to minimize the effect of small differences in absorption between samples. These differences in total absorption have consequences on bands associated with the buffer in the difference spectra (noted as * in the spectra). Therefore, interpretation of the FTIR data was limited to bands that were reproductively observed in spectra obtained with different samples.

Synchrotron-based analysis

UipA-uranyl complexes were prepared by mixing UipA proteins at 120 µM in 20 mM MES buffer 100 mM KCl pH 6 with uranyl 100 µM (stock solution of uranyl nitrate at 2.5 mM). Next, 200 µL of UipA-uranyl complexes were loaded in a kapton-teflon liquid cell for synchrotron analysis.

EXAFS data acquisition: experiments were performed on the MARS beamline at the SOLEIL synchrotron facility. Energy calibration was performed at the yttrium K edge at 17038 eV, and EXAFS experiments were conducted at the U L_{III} edge. The MARS beamline is dedicated to investigating radioactive materials in the hard X-ray range[14]. The beamline optics essentially consist of a water-cooled double-crystal monochromator (FMB Oxford), which is used to select the incident energy of the X-ray beam and for horizontal focalization, and two large water-cooled reflecting mirrors (IRELEC/SESO) that are used for high-energy rejection (harmonic part) and vertical collimation and focalization. All measurements were conducted in fluorescence mode using a 13-element high purity germanium detector (ORTEC) at room temperature.

EXAFS data processing was performed using the ATHENA code [15]. The E_0 energy was identified at the maximum of the absorption edge. Fourier transformation (FT) with k^2 weighting was performed between 2.8 and 11.8 $Å^{-1}$ with a Hanning window. The fits were performed using the DEMETER code (version Demeter 0.9.25) and were fit in R space between 1 and 5 Å. EXAFS data fitting: One global amplitude factor S_0^2 and one energy threshold correction factor ΔE_0 were used for every path of the fits. The agreement factor r (%) and the quality factor (QF = reduced χ^2) of the fits were provided directly by DEMETER. Phases and amplitudes were calculated using the FEFF6 simulation code integrated in DEMETER based on the structural model of uranyl-acetate complex ($UO_2(acetate)_2$ [16]. This model was chosen because it exhibits both monodentate and bidentate carboxylate ligation to the uranyl equatorial plane. The scattering paths used for the fitting procedure are: i) simple scattering paths including U-O_{ax} within the oxo bond, U-O_{eq} corresponding to the equatorial oxygen atoms, and U...C corresponding to the C atom of the bidentate carboxylate group; and ii) multiple scattering paths including the quadruple path U-O_{ax} within the oxo bond, and the triple scattering U-O-C of the monodentate carboxylate function. During the fitting procedure, the relative number of mono and bidentate carboxylates was allowed to fluctuate but the total number of O_{eq} was fixed to 5.

Statistical analyses

All measurements were performed at least in triplicate. The symbol ± corresponds to standard deviation.

1 Theodorakopoulos, N. *et al.* Use of combined microscopic and spectroscopic techniques to reveal interactions between uranium and Microbacterium sp A9, a strain isolated from the Chernobyl exclusion zone. *Journal of hazardous materials* **285**, 285-293, doi:10.1016/j.jhazmat.2014.12.018 (2015).
2 Gallois, N. *et al.* Proteogenomic insights into uranium tolerance of a Chernobyl's Microbacterium bacterial isolate. *Journal of proteomics* **177**, 148-157, doi:10.1016/j.jprot.2017.11.021 (2018).
3 Klein, G. *et al.* RNA-binding proteins are a major target of silica nanoparticles in cell extracts. *Nanotoxicology* **10**, 1555-1564, doi:10.1080/17435390.2016.1244299 (2016).
4 Ortet, P. *et al.* Complete Genome Sequences of Four Microbacterium Strains Isolated from Metal- and Radionuclide-Rich Soils. *Microbiology resource announcements* **8**, doi:10.1128/MRA.00846-19 (2019).
5 Dupierris, V., Masselon, C., Court, M., Kieffer-Jaquinod, S. & Bruley, C. A toolbox for validation of mass spectrometry peptides identification and generation of database: IRMa. *Bioinformatics* **25**, 1980-1981, doi:10.1093/bioinformatics/btp301 (2009).
6 Carvalho, P. C., Hewel, J., Barbosa, V. C. & Yates Iii, J. R. Identifying differences in protein expression levels by spectral counting and feature selection. *Genet Mol Res* **7**, 342-356 (2008).
7 Christie-Oleza, J. A., Fernandez, B., Nogales, B., Bosch, R. & Armengaud, J. Proteomic insights into the lifestyle of an environmentally relevant marine bacterium. *The ISME journal* **6**, 124-135, doi:10.1038/ismej.2011.86 (2012).
8 Perez-Riverol, Y. *et al.* The PRIDE database and related tools and resources in 2019: improving support for quantification data. *Nucleic Acids Res* **47**, D442-D450, doi:10.1093/nar/gky1106 (2019).
9 Karimova, G. & Ladant, D. Defining Membrane Protein Topology Using pho-lac Reporter Fusions. *Methods in molecular biology* **1615**, 129-142, doi:10.1007/978-1-4939-7033-9_10 (2017).
10 Bryksin, A. V. & Matsumura, I. Overlap extension PCR cloning: a simple and reliable way to create recombinant plasmids. *BioTechniques* **48**, 463-465, doi:10.2144/000113418 (2010).
11 Jiang, J. *et al.* Solution chemistry of uranyl ion with iminodiacetate and oxydiacetate: a combined NMR/EXAFS and potentiometry/calorimetry study. *Inorganic Chemistry* **42**, 1233-1240 (2003).
12 Smith, R. M. & Martell, A. E. *Critical stability constants: second supplement*. (Springer, 1989).
13 Maeder, M. & King, P. (Jplus Consulting Pty Ltd East Fremantle, West Australia, Australia, 2009).
14 LLorens, I. *et al.* X-ray absorption spectroscopy investigations on radioactive matter using MARS beamline at SOLEIL synchrotron. *Radiochimica Acta* **102**, 957-972, doi:10.1515/ract-2013-2241 (2014).
15 Ravel, B. & Newville, M. ATHENA, ARTEMIS, HEPHAESTUS: data analysis for X-ray absorption spectroscopy using IFEFFIT. *J Synchrotron Radiat* **12**, 537-541, doi:10.1107/S0909049505012719 (2005).
16 Howatson, J., Grev, D. M. & Morosin, B. Crystal and Molecular-Structure of Uranyl Acetate Dihydrate. *J Inorg Nucl Chem* **37**, 1933-1935, doi:Doi 10.1016/0022-1902(75)80918-3 (1975).

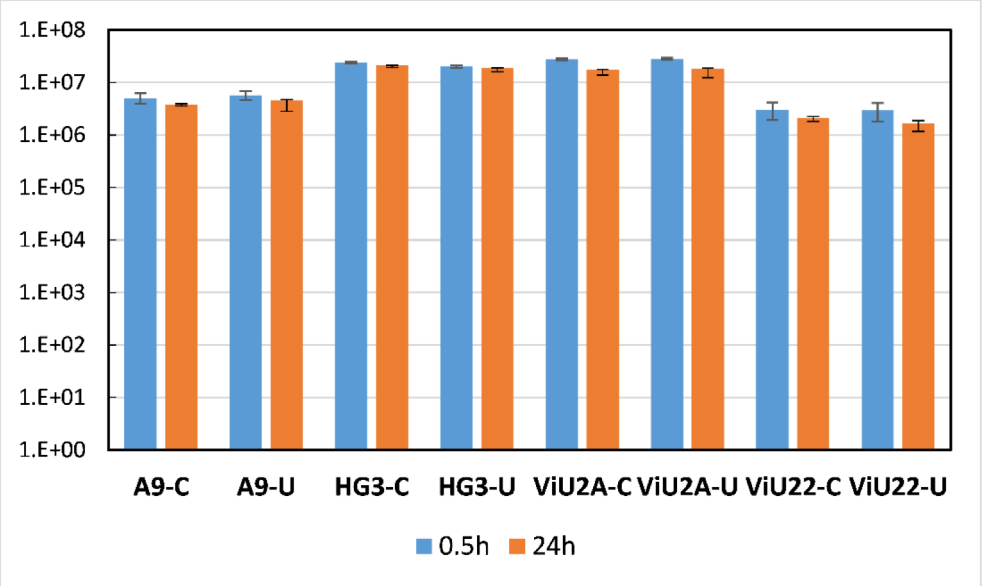

Fig. S1. Cell viability at 0.5h and 24h of exposure to 0 µM (C) and 10 µM uranyl (U) at 25°C for strains A9, HG3, ViU2A and ViU22.

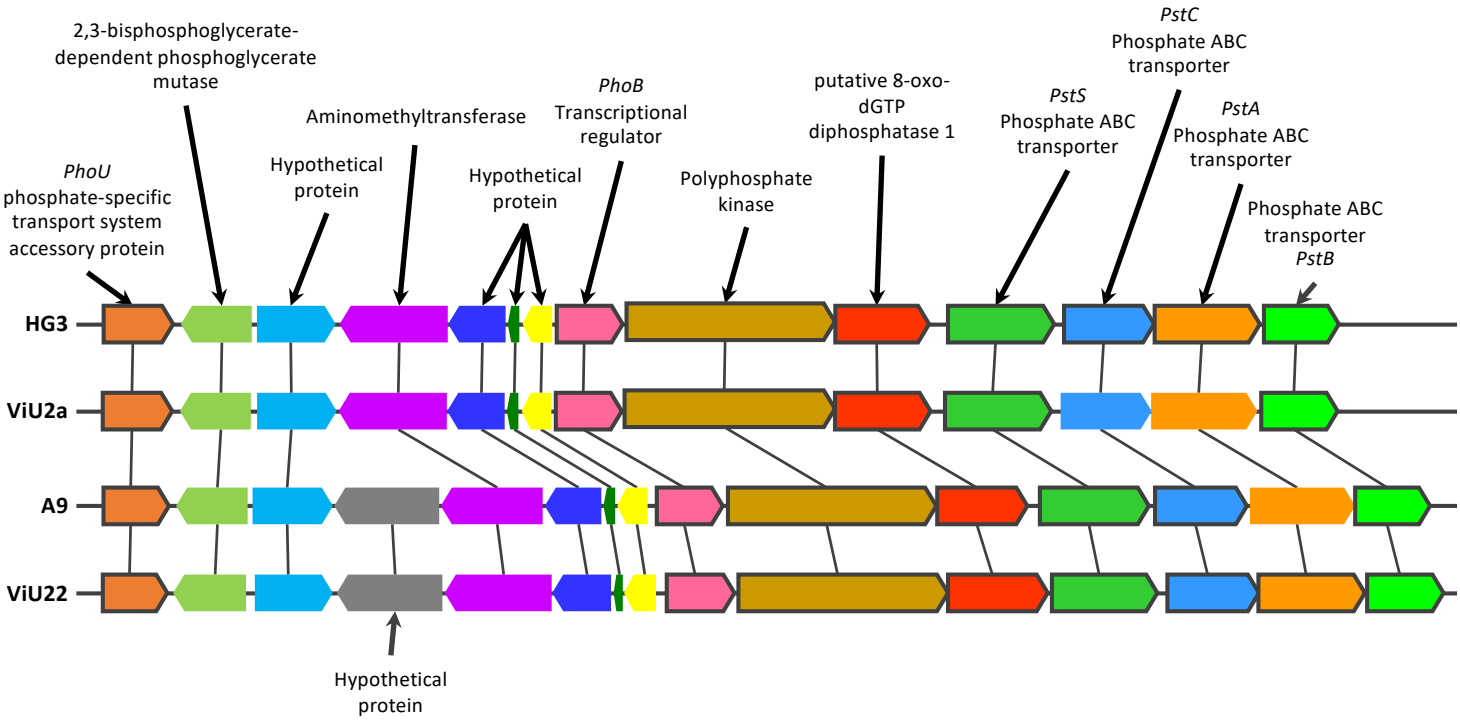

Fig. S2. genomic organization of *phoU*, *phoB* and *pstSCAB* genes in *Microbacterium* sp. strains. Genes with a marked outline are coding for proteins which are modulated by uranium.

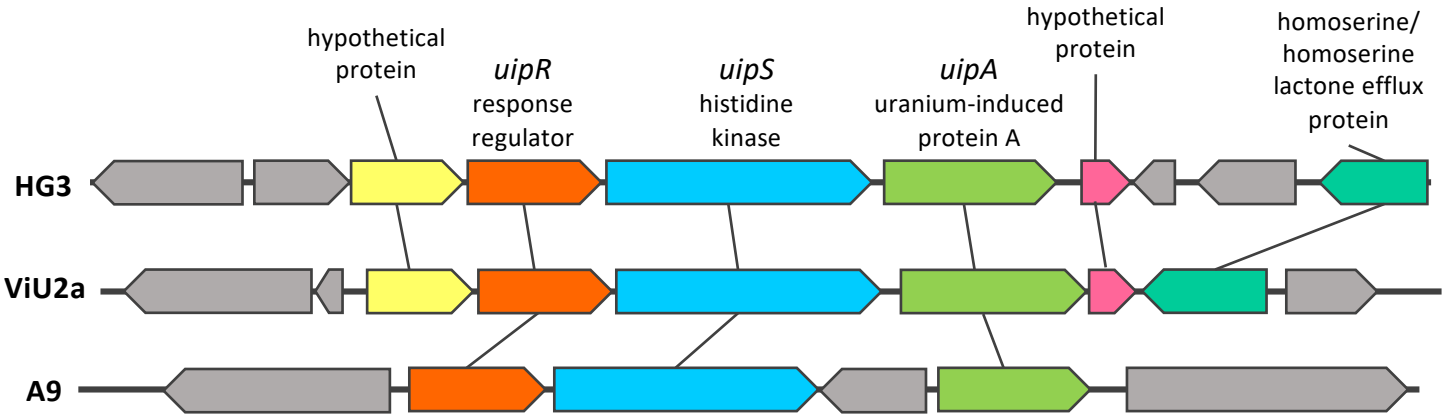

A. Synteny of the *uipR, S and A* genes in *Microbacterium* sp. strains ViU2A, HG3 and A9.

	Gene	Length (aa)	Mw (kDa)	pI	Charged residues (%)	Predicted topology (aa number)		% id with ViU2A	% id with HG3	% id with A9
						inside	outside			
$UipA_{ViU2A}$	CVS53_03692	281	28.1	3.86	19.9	1 to 71	95 to 281	100	74.6	36.6
$UipA_{HG3}$	CVS54_03678	285	28.3	3.89	20.7	1 to 75	99 to 285		100	36.7
$UipA_{A9}$	BWL13_02796	247	24.8	3.99	18.6	1 to 38	62 to 247			100

B. Characteristics of UipA proteins

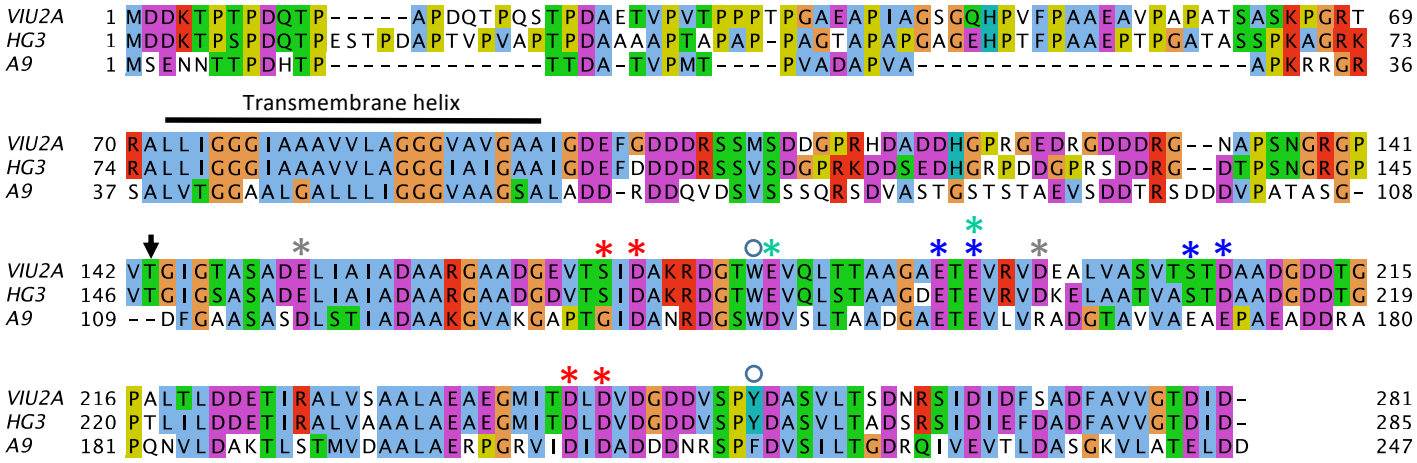

C. Multiple sequence alignment of the full-length UipA proteins visualized in Jalview. Amino acids involved in U coordination as deduced from the crystallographic structure are marked with blue (U1 site), green (U2 site), red (U3 site) and grey (U4 site) stars. The first residue seen in the electron density is marked with an arrow and the position of fluorescent residues (W and Y) is marked with open circles.

Fig. S3. Genomic context of *uipA* genes and sequence analysis of UipA proteins

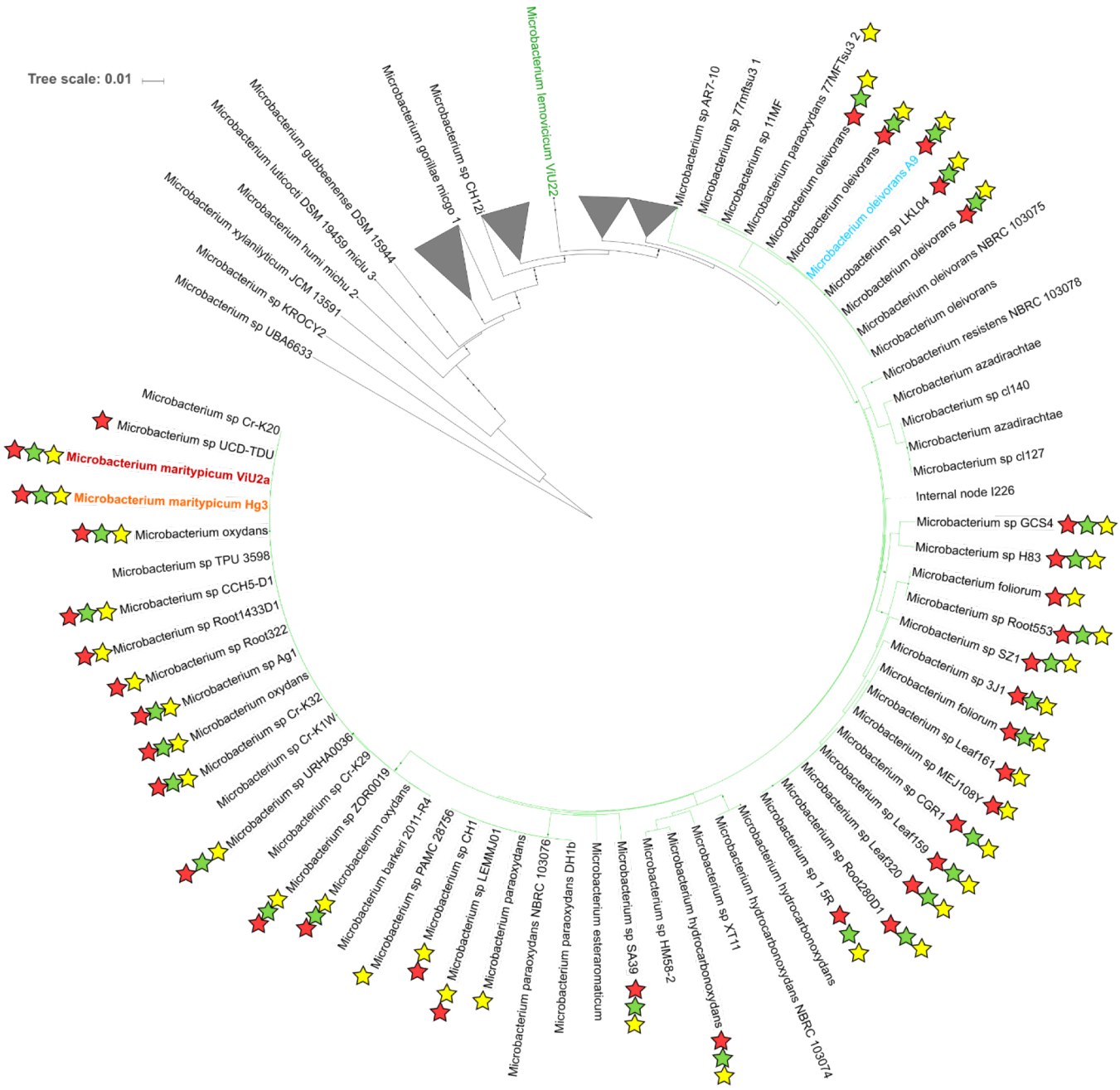

Fig. S4. Phylogenetic tree constructed with 16SrRNA genes of *Microbacterium* sp. whose genome sequences are available in Genbank (draft or complete). For each strain, the presence of *uipA, uipR* and *uipS* genes is indicated by a yellow, green and red star respectively.

A

MDDKTPTPDQTPAPDQTPQSTPDAETVPVTPPPTPGAEAPIAGSGQHPVFPAAEAVPAPATSASKPGRTRALLIGGGIAAAVVL
AGGGVAVGAAIGDEFGDDDRSSMSDDGPRHDADDHGPRGEDRGDDDRGNAPSNGRGPVTGIGTASADELIAIADAARGAA
DGEVTSIDAKRDGTWEVQLTTAAGAETEVRVDEALVASVTSTDAADGDDTGPALTLDDETIRALVSAALAEAEGMITDLDVDGD
DVSPYDASVLTSDNRSIDIDFSADFAVVGTDID

B

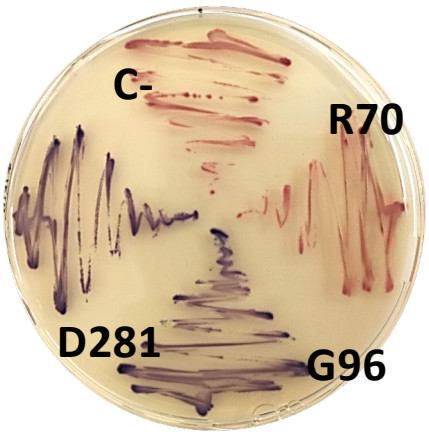

Fig. S5. UipA$_{ViU2A}$ topology analysis. A. Hypothetical topology model of UipA derived from the CCTOP prediction: the transmembrane segment is highlighted in grey, the intracellular and extracellular segments are in green and yellow, respectively. Small circles indicate insertion positions of the dual PhoA-LacZα fusion reporter in frame with the codons corresponding to the amino acid residues R70, G96 and D281. B. Experimental validation of UipA membrane topology: *E. coli* DH5α cells expressing the constructed UipA-Pho-LacZα fusions were streaked on the LB double indicator plate. Blue color indicates a high alkaline phosphatase activity and a periplasmic location of the fusion point, when red color indicates a high β-galactosidase activity and a cytoplasmic location of the fusion point. A negative control (c-) is performed with the Pho-LacZα reporter without insertion.

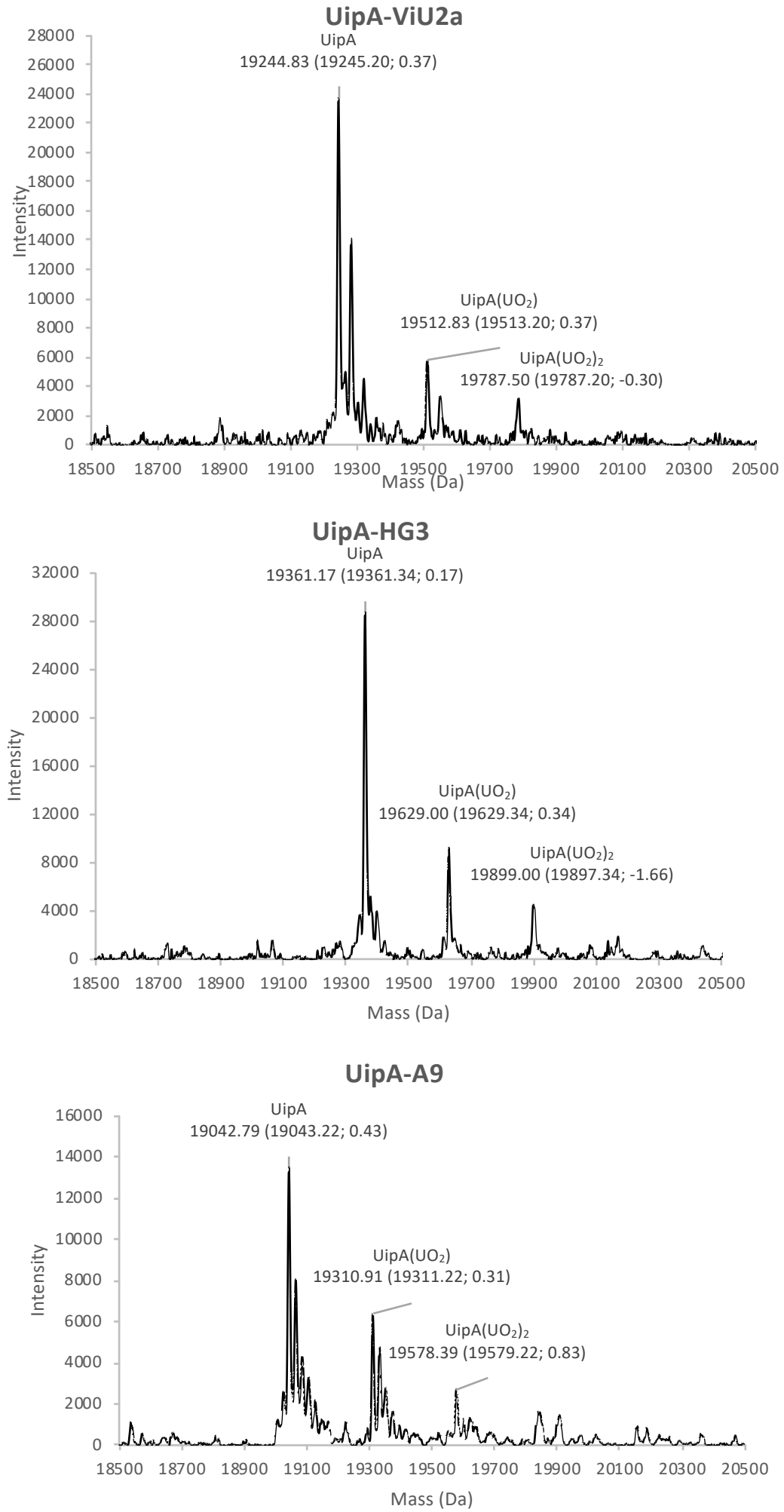

Fig. S6. native mass spectra obtained with $UipA_{ext}$ peptides and UO_2^{2+}. For each complex, the observed neutral average is indicated as well as the theorical neutral average mass and the deviation between theorical and observed mass (in brackets).

ViU2A – UO_2^{2+}

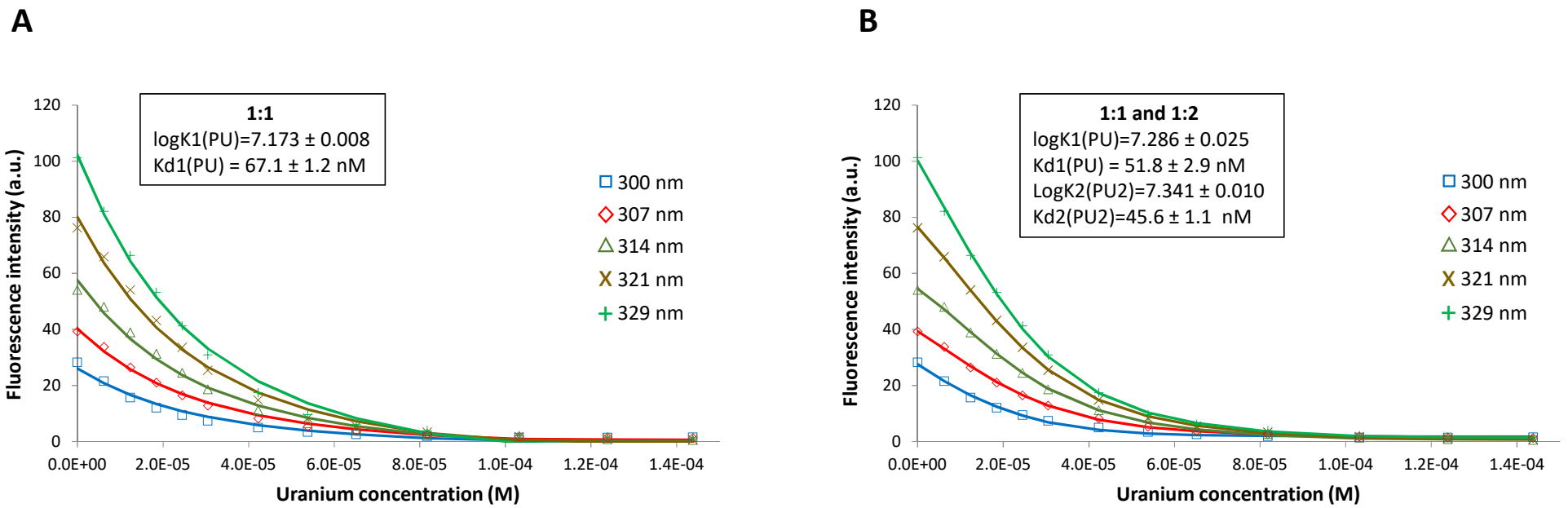

Fig. S7: Fitting curves for $UipA_{ext}$-ViU2A protein and UO_2^{2+} complexes formation measured by fluorescence titration. Experimental data (symbols) and fitting curves (continuous lines) obtained at different wavelength as indicated in the legend with the assumption of A) 1:1 and B)1:1 and 1:2 protein-metal complexes formation. The parameters (log K1/K2 and Kd) calculated with Reactlab are indicated for each scenario.

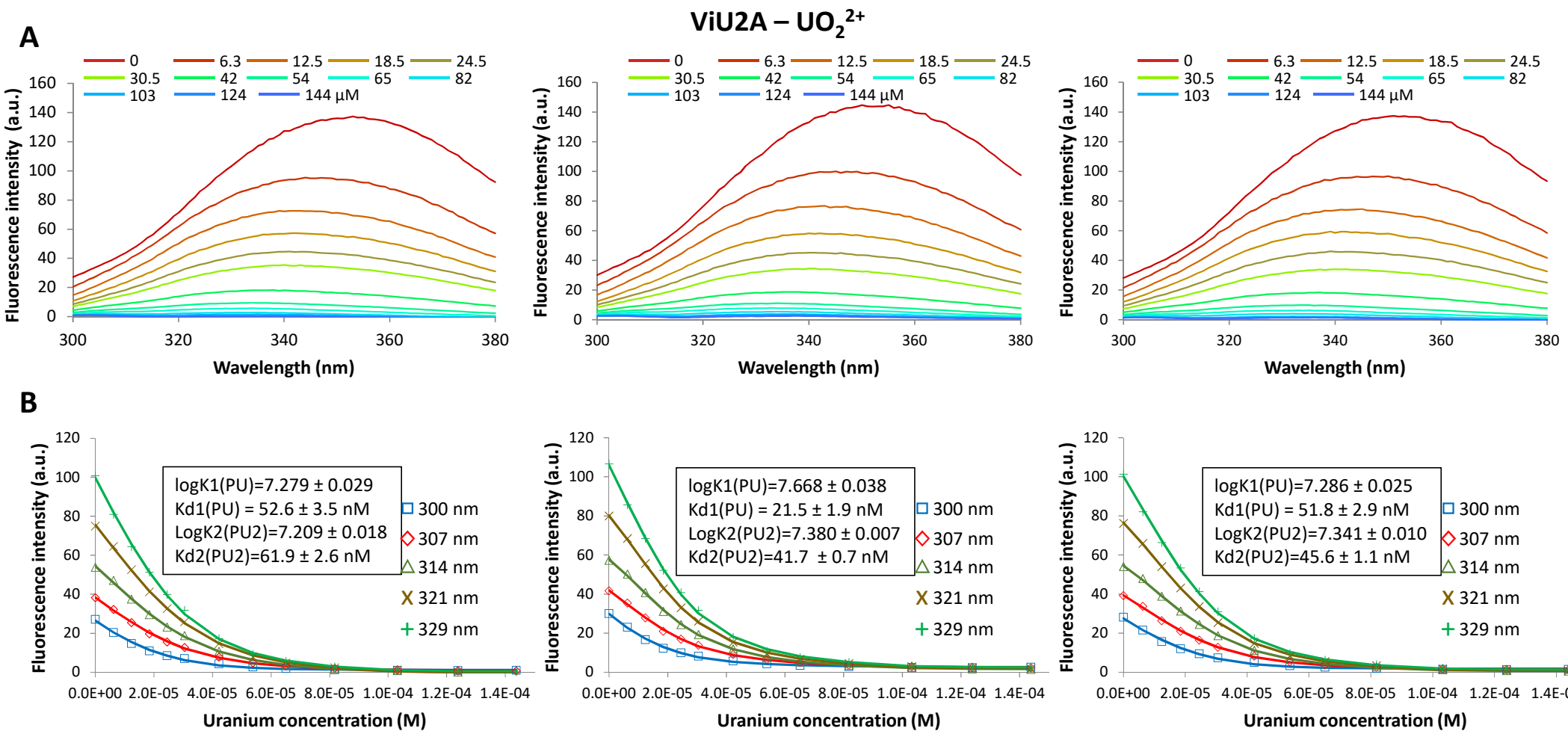

Fig. S8: Fluorescence spectra and fitting curves obtained with $UipA_{ext}$-ViU2A protein and UO_2^{2+} in a triplicate experiment. A) Fluorescence spectra recorded between 300 and 380 nm with different uranium concentrations (given in µM in the legend). B) Experimental data (symbols) and fitting curves (continuous lines) obtained at different wavelength as indicated in the legend with the assumption of 1:1 and 1:2 protein metal complexes formation. For each replicate, logK1(1:1 protein metal complex), logK2(1:2 protein metal complex) and the dissociation constant ($Kd=1/10^{logK}$) calculated in Reactlab are indicated.

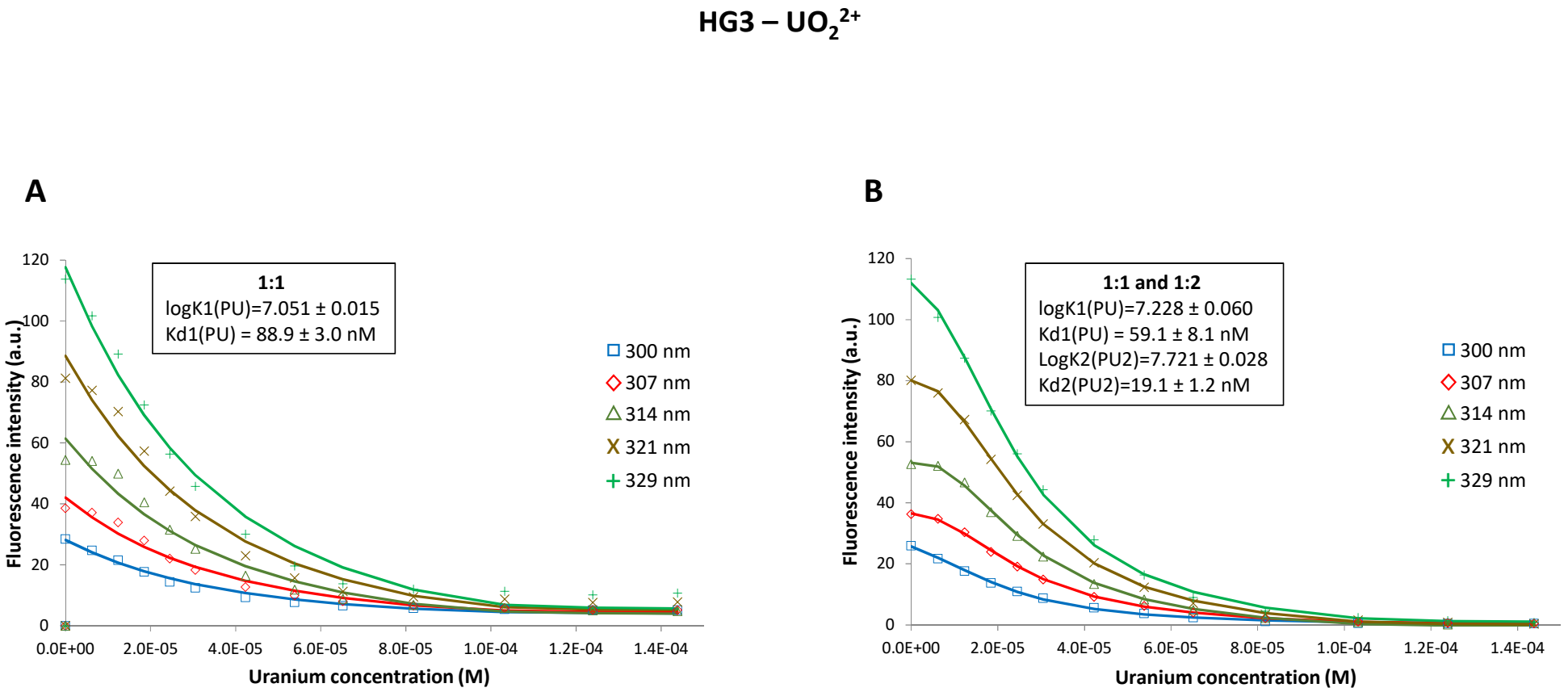

Fig. S9: Fitting curves $UipA_{ext}$-HG3 protein and UO_2^{2+} complexes formation measured by fluorescence titration. Experimental data (symbols) and fitting curves (continuous lines) obtained at different wavelength as indicated in the legend with the assumption of A) 1:1 and B)1:1 and 1:2 protein-metal complexes formation. The parameters (log K1/K2 and Kd) calculated with Reactlab are indicated for each scenario.

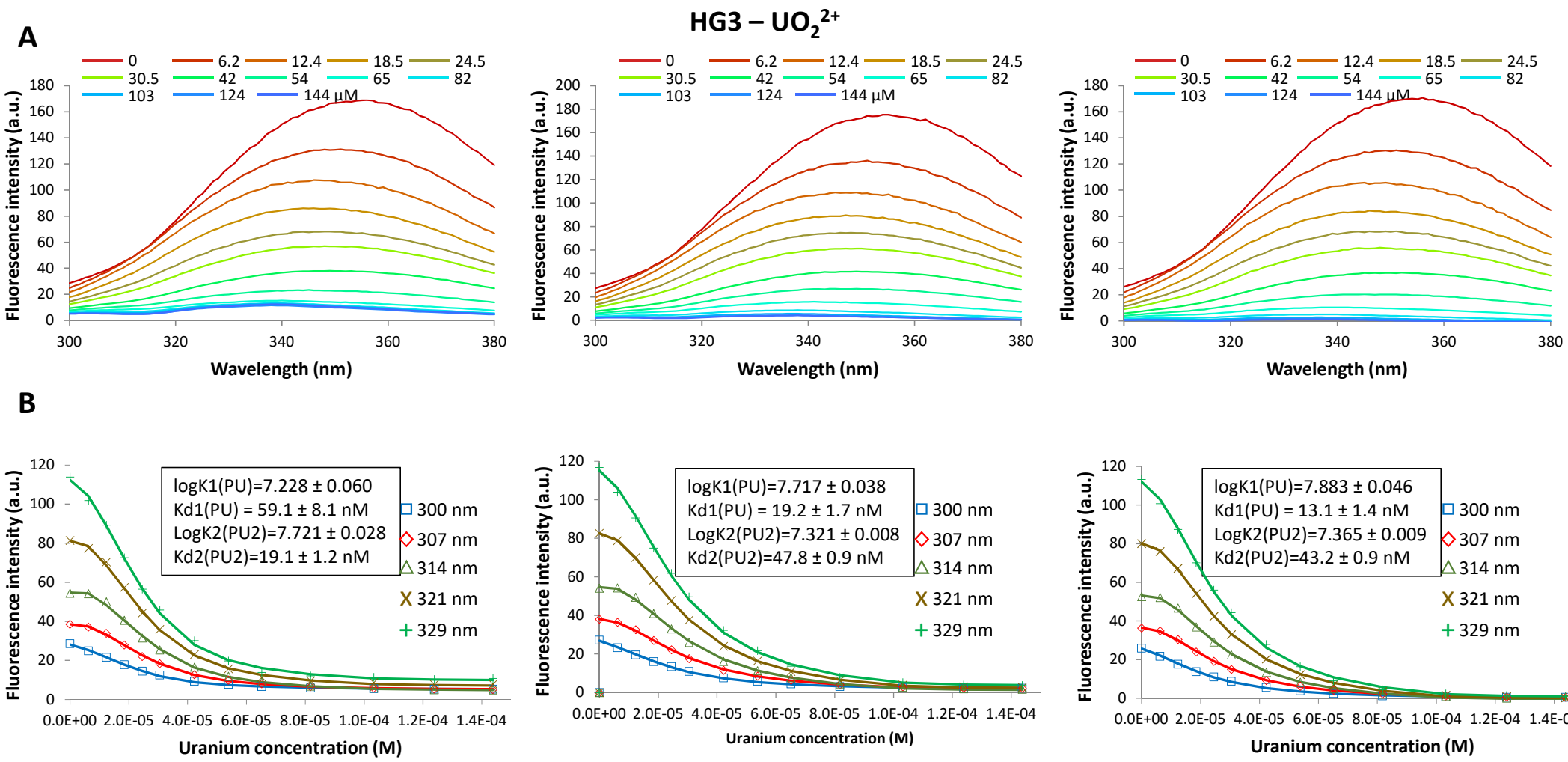

Fig. S10: Fluorescence spectra and fitting curves obtained with UipA$_{ext}$-HG3 protein and UO_2^{2+} in a triplicate experiment. A) Fluorescence spectra recorded between 300 and 380 nm with different uranium concentrations (given in µM in the legend). B) Experimental data (symbols) and fitting curves (continuous lines) obtained at different wavelength as indicated in the legend with the assumption of 1:1 and 1:2 protein metal complexes formation. For each replicate, logK1(1:1 protein metal complex), logK2(1:2 protein metal complex) and the dissociation constant ($Kd=1/10^{logK}$) calculated in Reactlab are indicated.

A9 – UO_2^{2+}

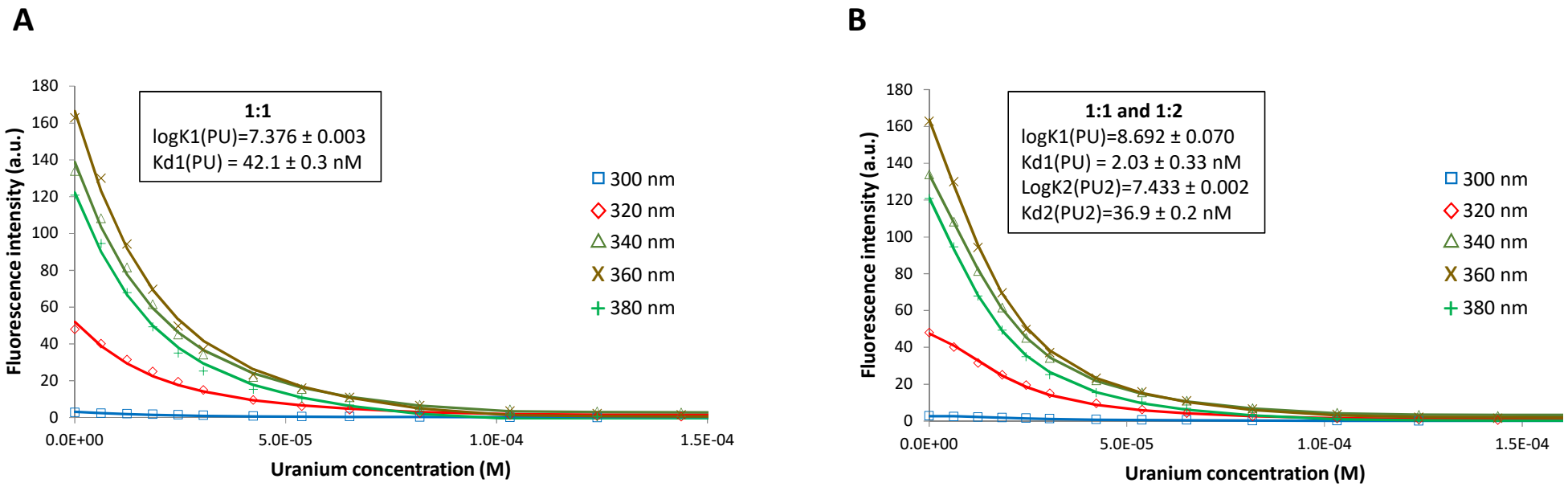

Fig. S11: Fitting curves for $UipA_{ext}$-A9 protein and UO_2^{2+} complexes formation measured by fluorescence titration. Experimental data (symbols) and fitting curves (continuous lines) obtained at different wavelength as indicated in the legend with the assumption of A) 1:1 and B)1:1 and 1:2 protein-metal complexes formation. The parameters (log K1/K2 and Kd) calculated with Reactlab are indicated for each scenario.

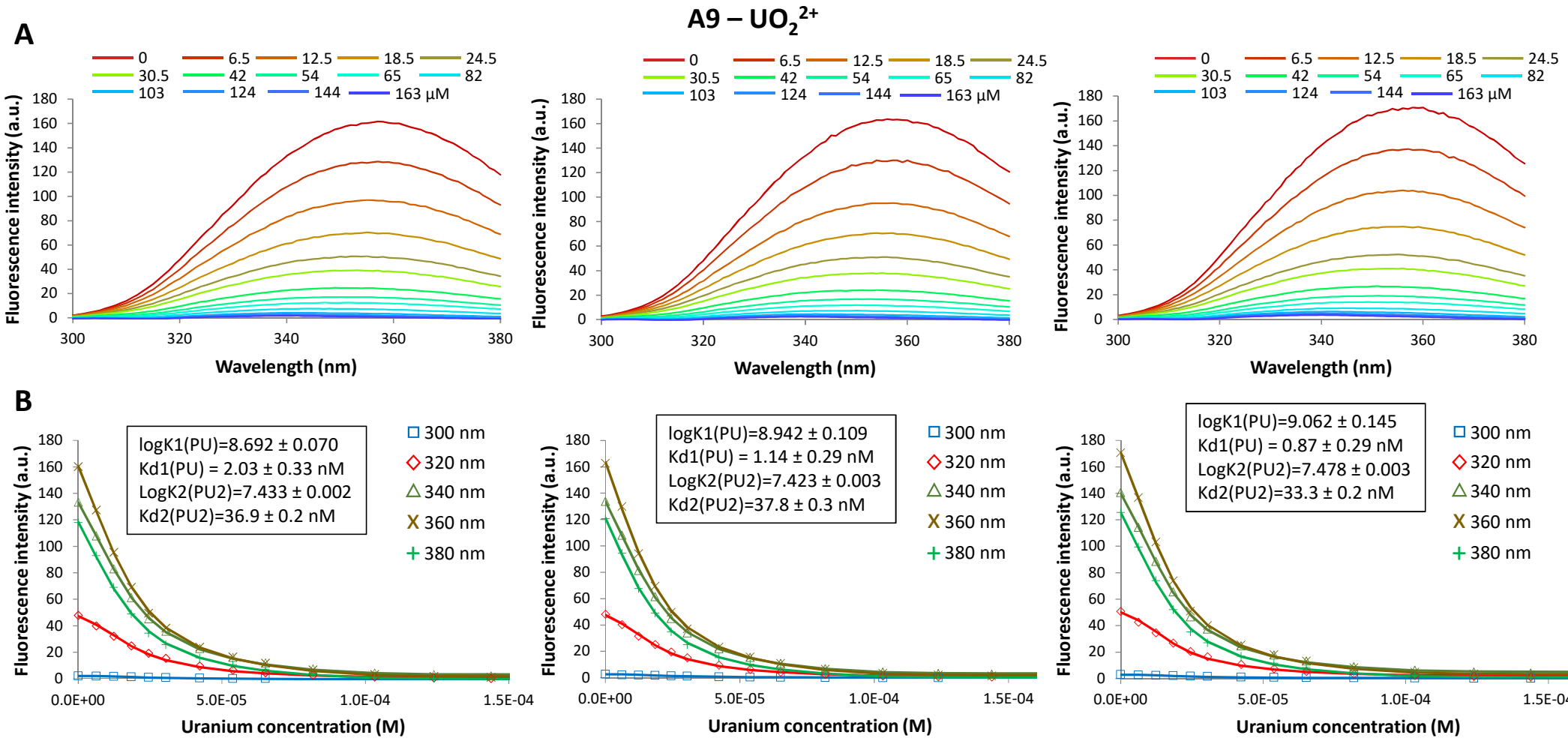

Fig. S12: Fluorescence spectra and fitting curves obtained with UipA$_{ext}$-A9 protein and UO_2^{2+} in a triplicate experiment. A) Fluorescence spectra recorded between 300 and 380 nm with different uranium concentrations (given in µM in the legend). B) Experimental data (symbols) and fitting curves (continuous lines) obtained at different wavelength as indicated in the legend with the assumption of 1:1 and 1:2 protein metal complexes formation. For each replicate, logK1(1:1 protein metal complex), logK2(1:2 protein metal complex) and the dissociation constant ($Kd=1/10^{logK}$) calculated in Reactlab are indicated.

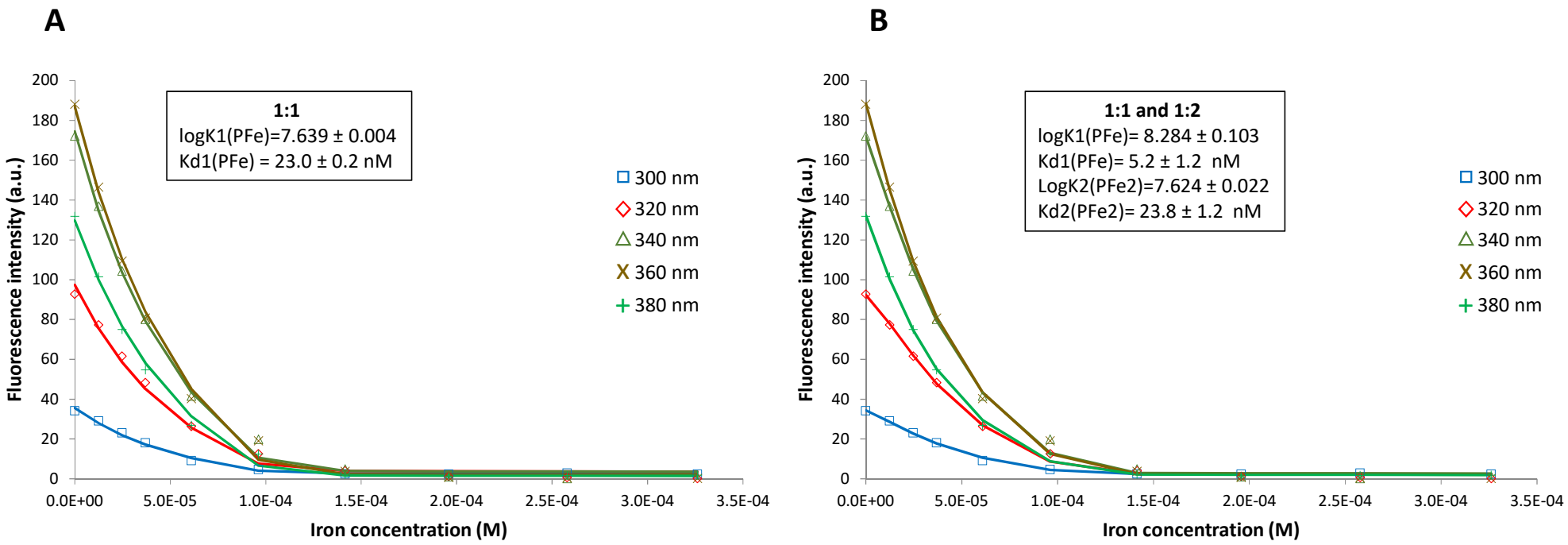

Fig. S13: Fitting curves for $UipA_{ext}$-ViU2A protein and Fe^{3+} complexes formation measured by fluorescence titration. Experimental data (symbols) and fitting curves (continuous lines) obtained at different wavelength as indicated in the legend with the assumption of A) 1:1 and B)1:1 and 1:2 protein-metal complexes formation. The parameters (log K1/K2 and Kd) calculated with Reactlab are indicated for each scenario.

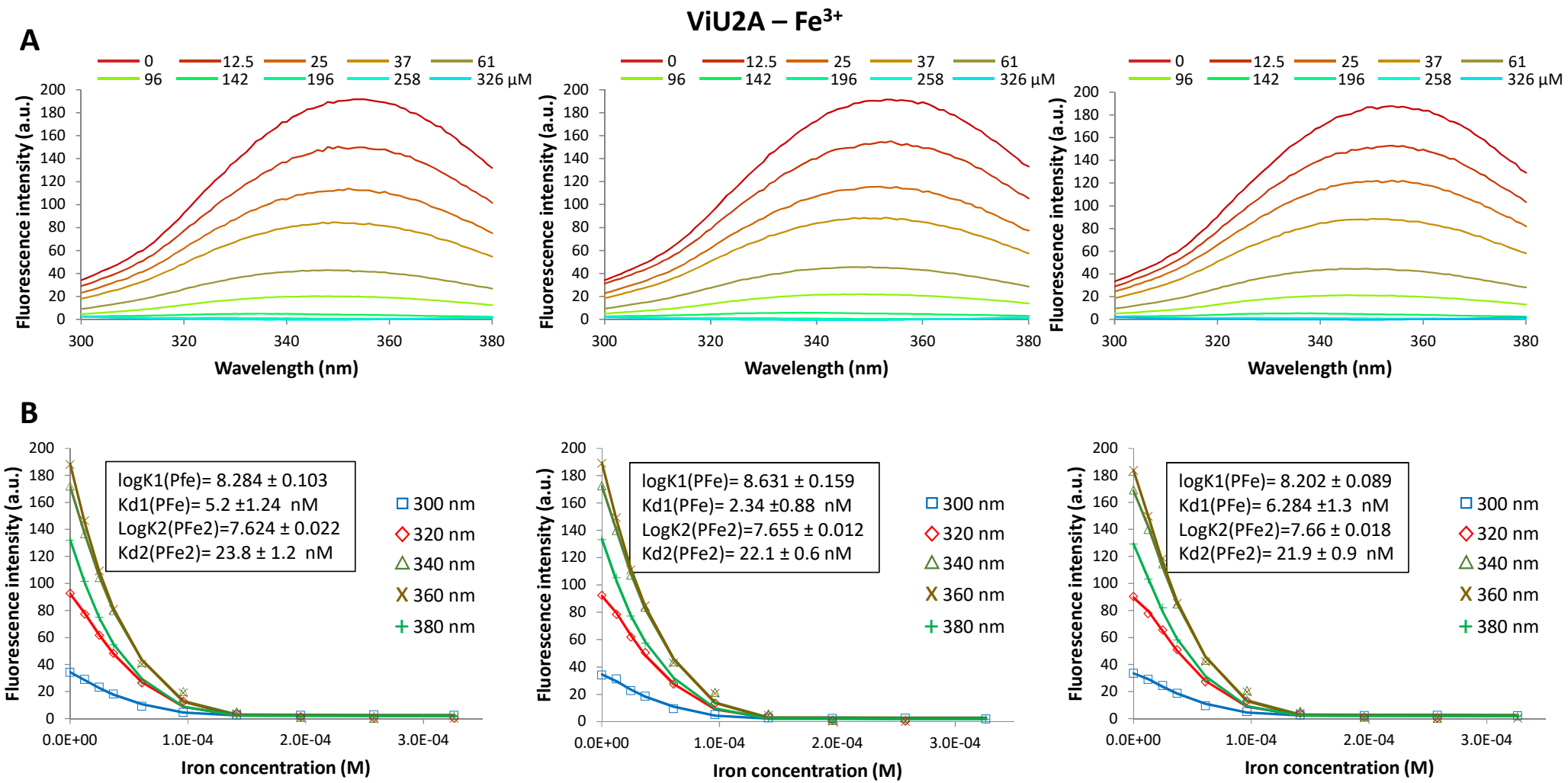

Fig. S14: Fluorescence spectra and fitting curves obtained with $UipA_{ext}$-ViU2A protein and Fe^{3+} in a triplicate experiment . A) Fluorescence spectra recorded between 300 and 380 nm with different iron concentrations (given in µM in the legend). B) Experimental data (symbols) and fitting curves (continuous lines) obtained at different wavelength as indicated in the legend with the assumption of 1:1 and 1:2 protein metal complexes formation. For each replicate, logK1(1:1 protein metal complex), logK2(1:2 protein metal complex) and the dissociation constant ($Kd=1/10^{logK}$) calculated in Reactlab are indicated.

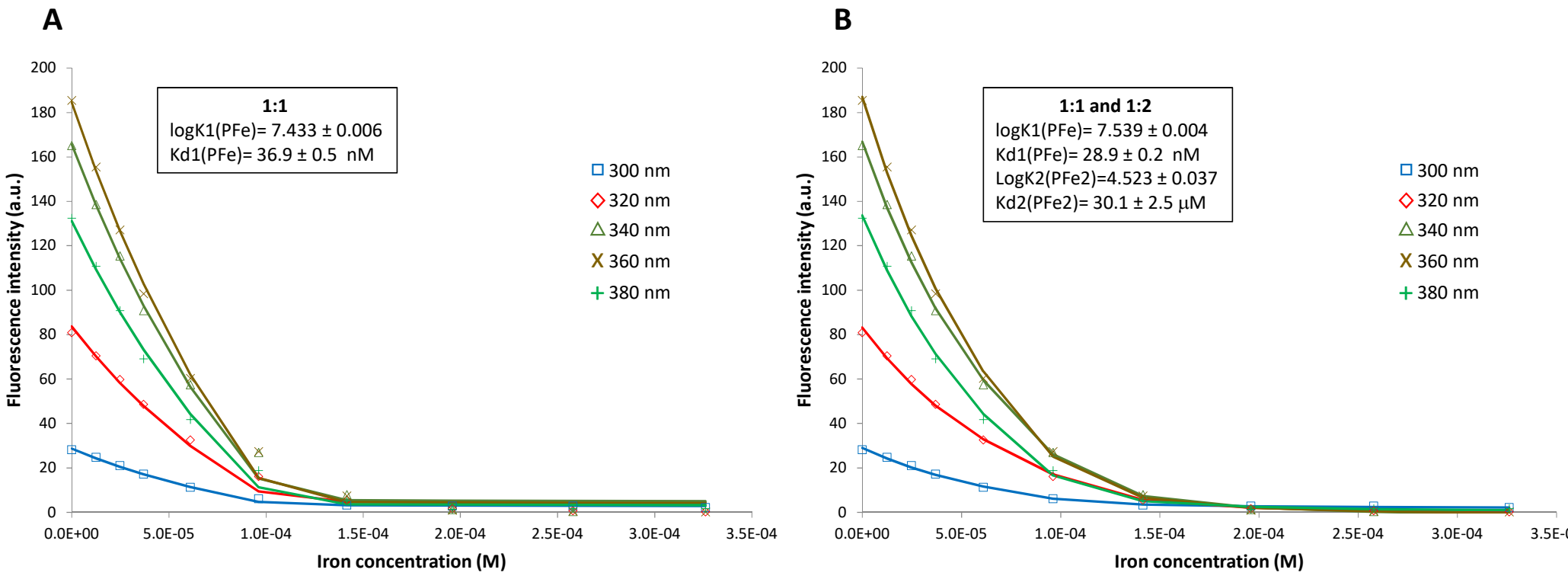

Fig. S15: Fitting curves for $UipA_{ext}$-HG3 protein and Fe^{3+} complexes formation measured by fluorescence titration. Experimental data (symbols) and fitting curves (continuous lines) obtained at different wavelength as indicated in the legend with the assumption of A) 1:1 and B)1:1 and 1:2 protein-metal complexes formation. The parameters (log K1/K2 and Kd) calculated with Reactlab are indicated for each scenario.

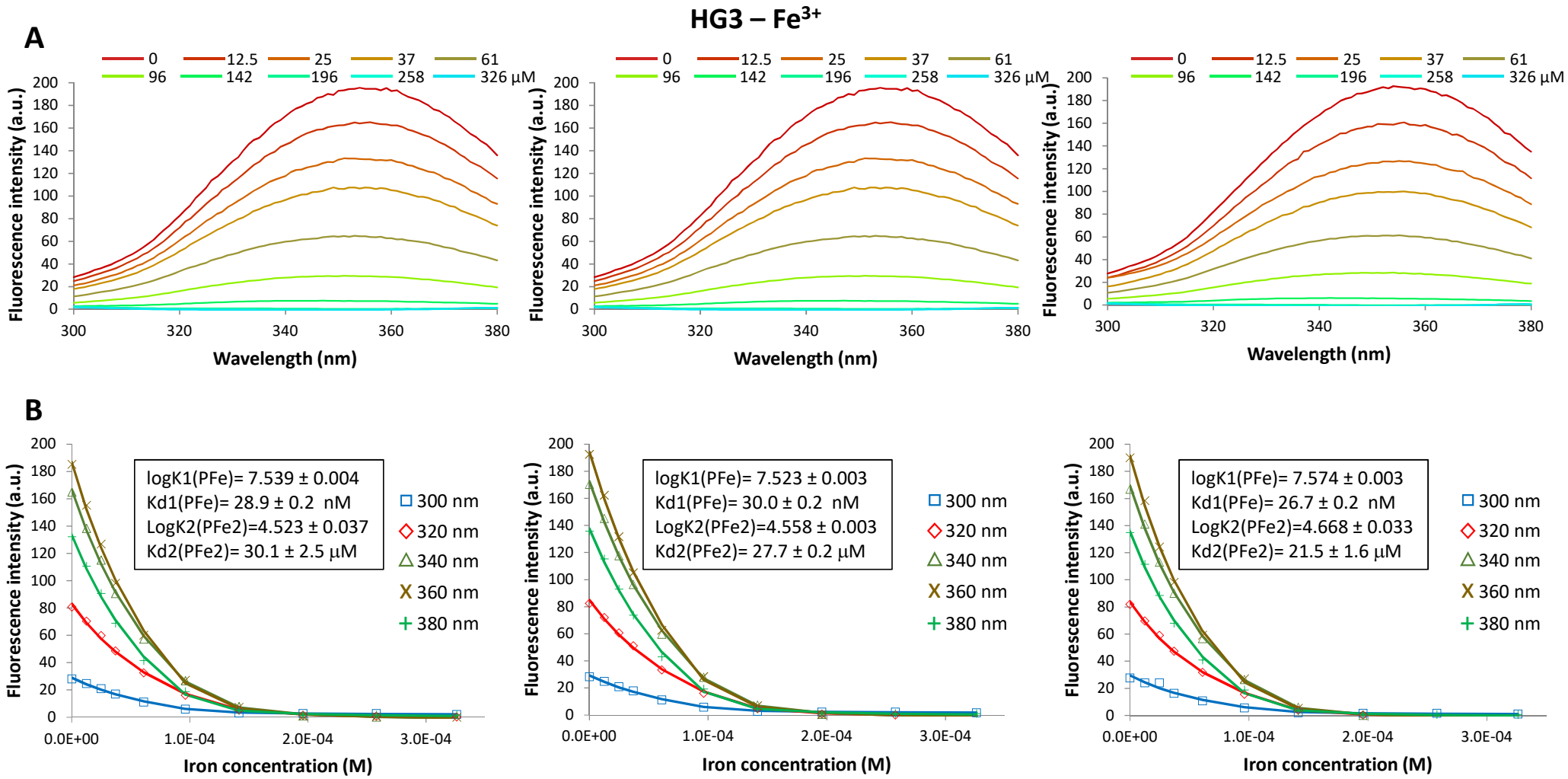

Fig. S16: Fluorescence spectra and fitting curves obtained with $UipA_{ext}$-HG3 protein and Fe^{3+} in a triplicate experiment. A) Fluorescence spectra recorded between 300 and 380 nm with different iron concentrations (given in µM in the legend). B) Experimental data (symbols) and fitting curves (continuous lines) obtained at different wavelength as indicated in the legend with the assumption of 1:1 and 1:2 protein metal complexes formation. For each replicate, logK1(1:1 protein metal complex), logK2(1:2 protein metal complex) and the dissociation constant ($Kd=1/10^{logK}$) calculated in Reactlab are indicated.

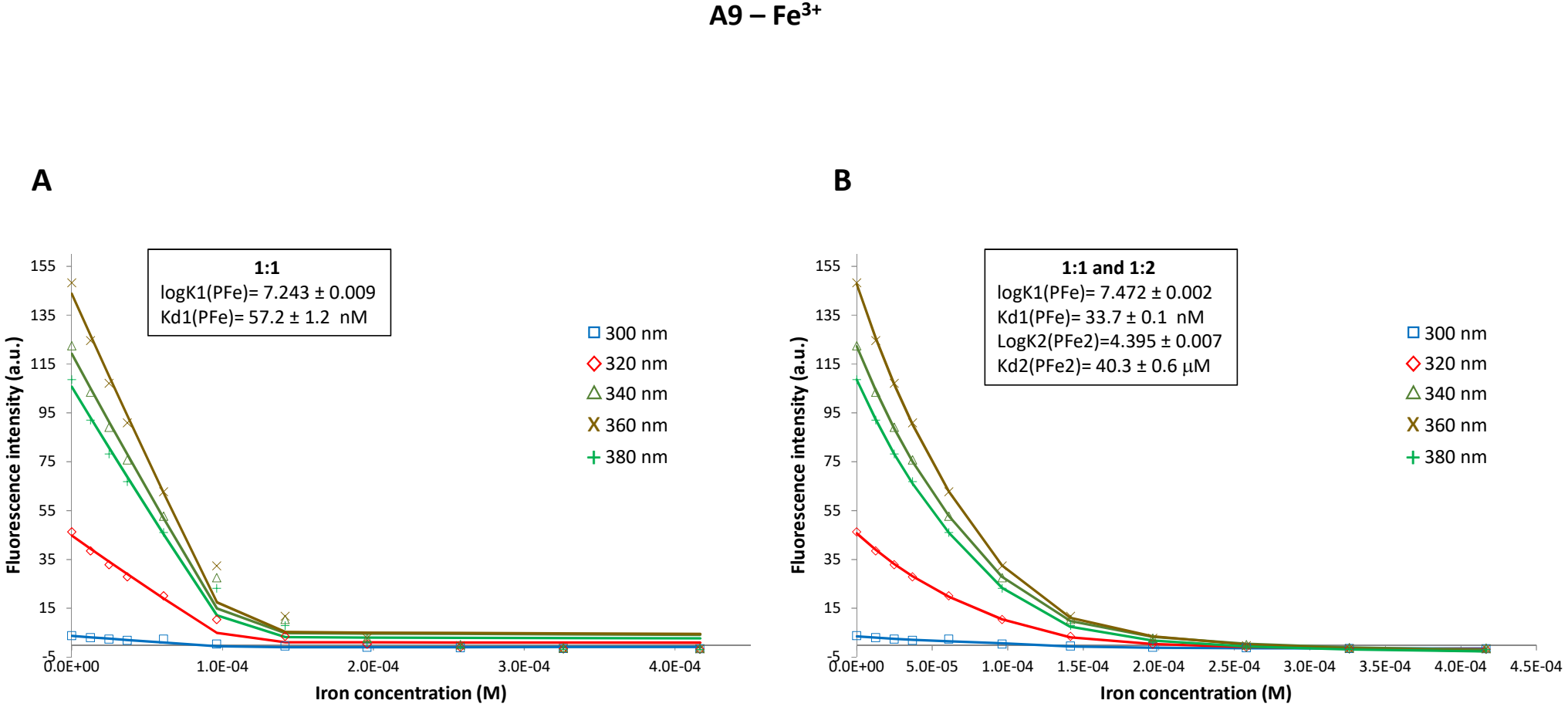

Fig. S17: Fitting curves for $UipA_{ext}$-A9 protein and Fe^{3+} complexes formation measured by fluorescence titration. Experimental data (symbols) and fitting curves (continuous lines) obtained at different wavelength as indicated in the legend with the assumption of A) 1:1 and B)1:1 and 1:2 protein-metal complexes formation. The parameters (log K1/K2 and Kd) calculated with Reactlab are indicated for each scenario.

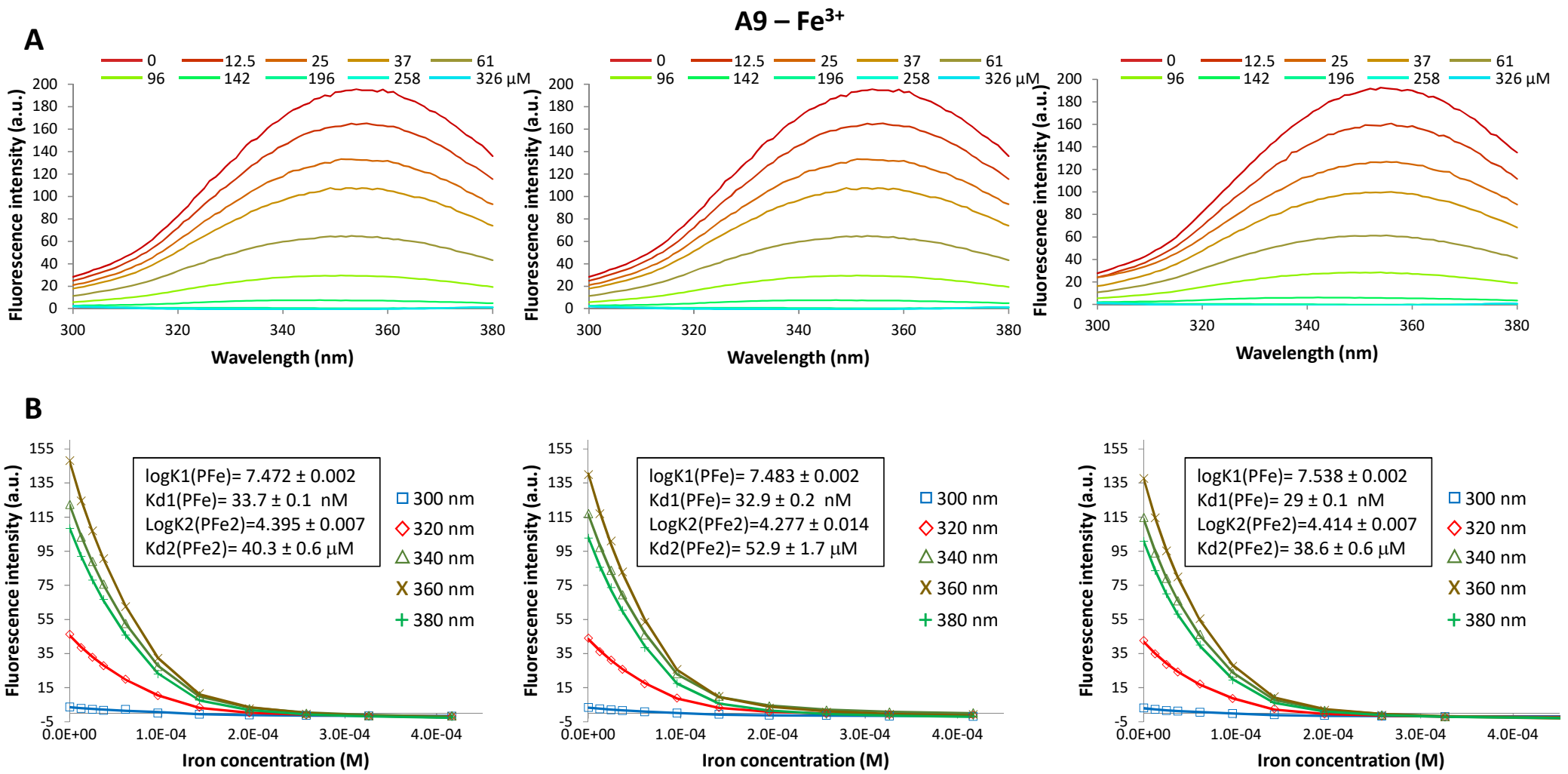

Fig. S18: Fluorescence spectra and fitting curves obtained with $UipA_{ext}$-A9 protein and Fe^{3+} in a triplicate experiment. A) Fluorescence spectra recorded between 300 and 380 nm with different iron concentrations (given in µM in the legend). B) Experimental data (symbols) and fitting curves (continuous lines) obtained at different wavelength as indicated in the legend with the assumption of 1:1 and 1:2 protein metal complexes formation. For each replicate, logK1(1:1 protein metal complex), logK2(1:2 protein metal complex) and the dissociation constant ($Kd=1/10^{logK}$) calculated in Reactlab are indicated.

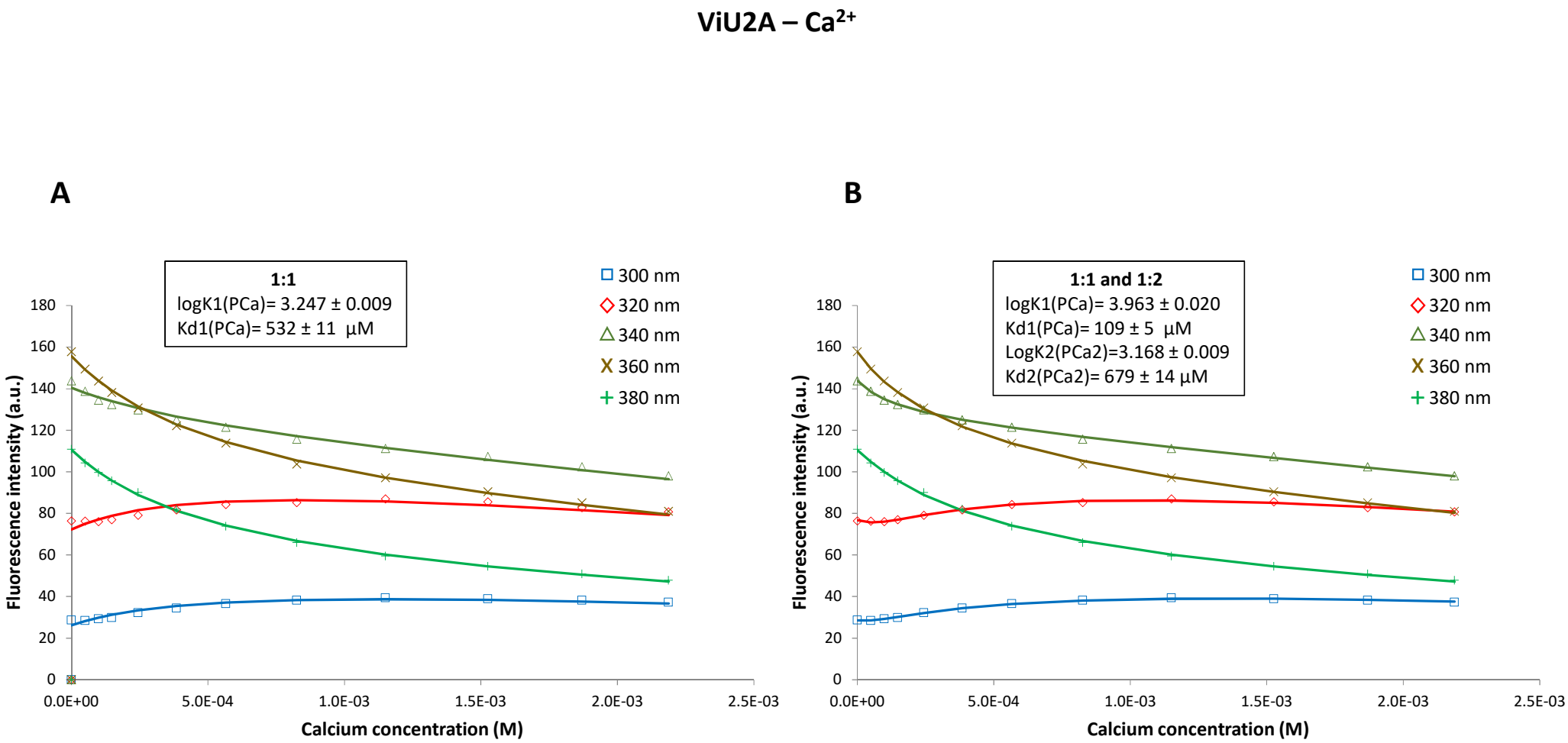

Fig. S19: Fitting curves for $UipA_{ext}$-ViU2A protein and Ca^{2+} complexes formation measured by fluorescence titration. Experimental data (symbols) and fitting curves (continuous lines) obtained at different wavelength as indicated in the legend with the assumption of A) 1:1 and B)1:1 and 1:2 protein-metal complexes formation. The parameters (log K1/K2 and Kd) calculated with Reactlab are indicated for each scenario.

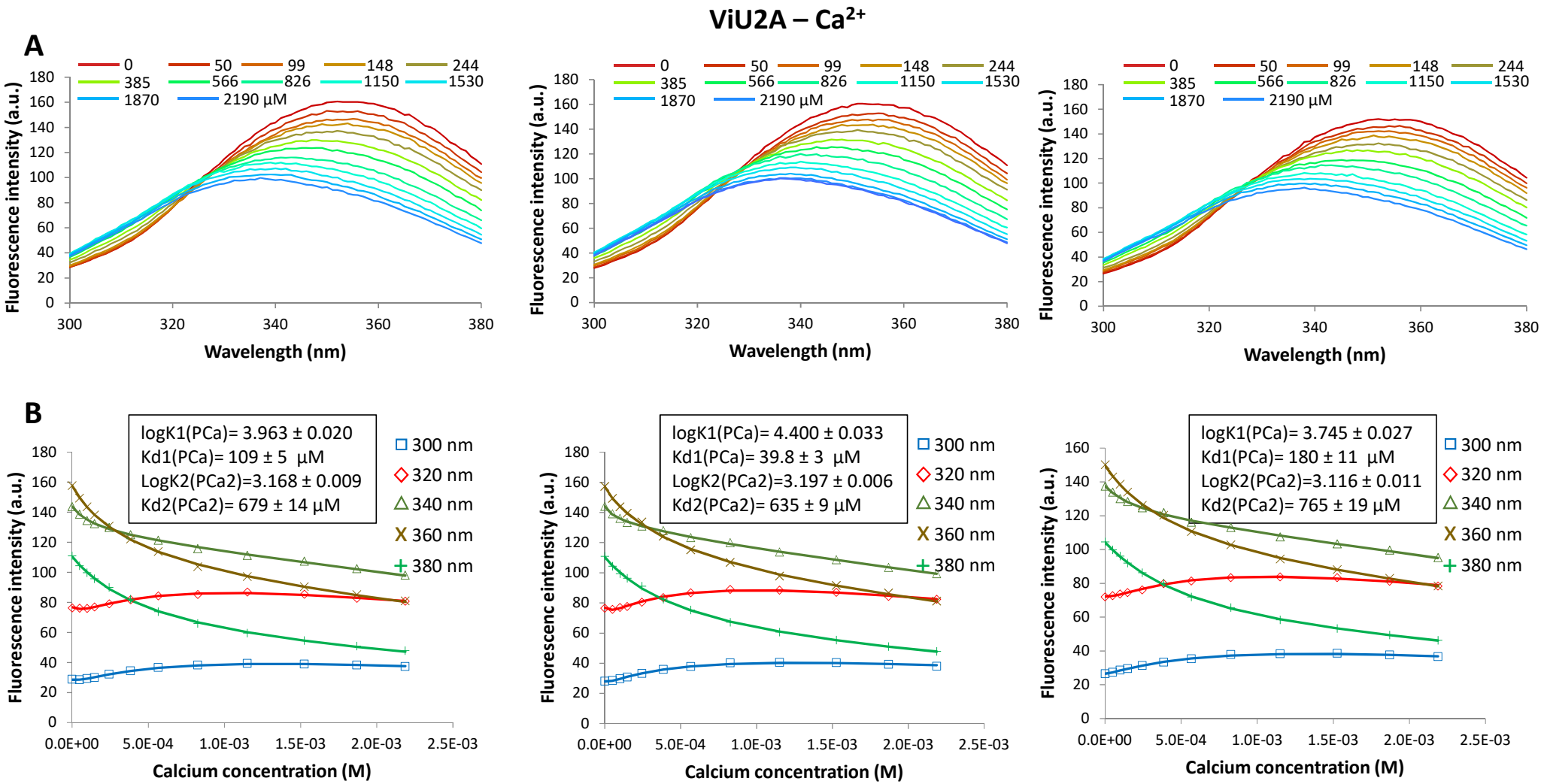

Fig. S20: Fluorescence spectra and fitting curves obtained with $UipA_{ext}$-ViU2A protein and Ca^{2+} in a triplicate experiment. A) Fluorescence spectra recorded between 300 and 380 nm with different calcium concentrations (given in µM in the legend). B) Experimental data (symbols) and fitting curves (continuous lines) obtained at different wavelength as indicated in the legend with the assumption of 1:1 and 1:2 protein metal complexes formation. For each replicate, logK1(1:1 protein metal complex), logK2(1:2 protein metal complex) and the dissociation constant ($Kd=1/10^{logK}$) calculated in Reactlab are indicated.

HG3 – Ca^{2+}

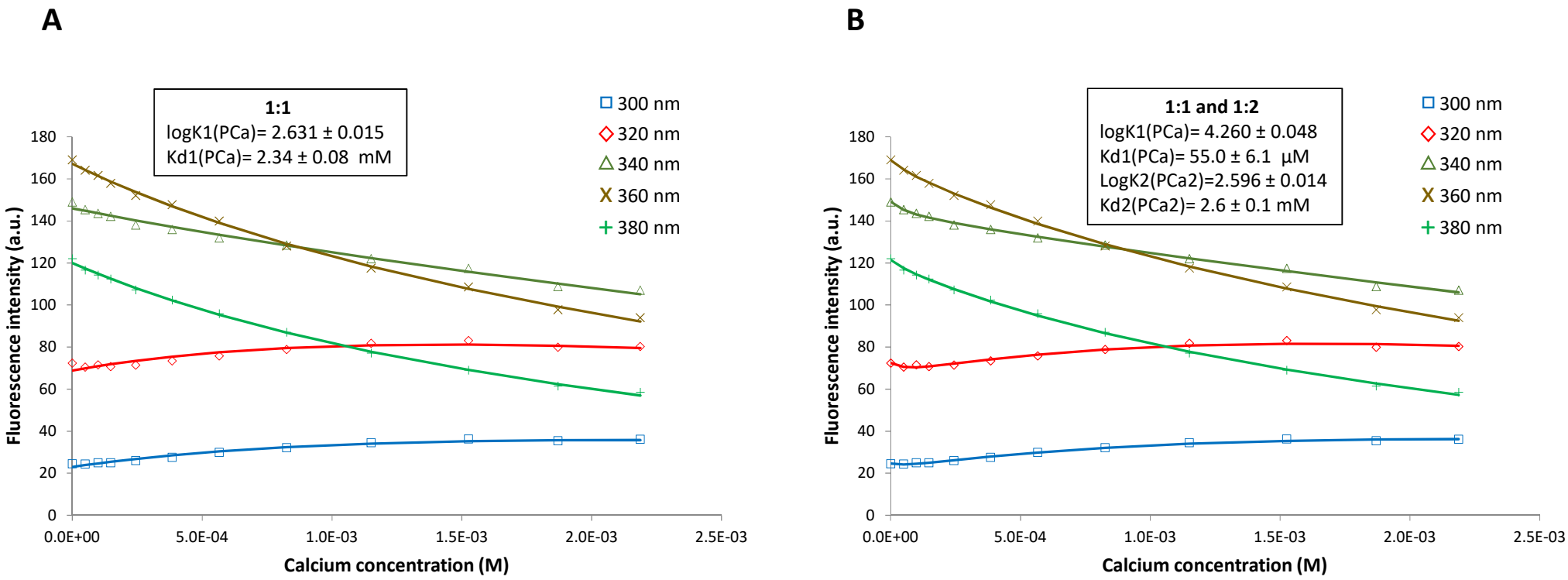

Fig. S21: Fitting curves for $UipA_{ext}$-HG3 protein and Ca^{2+} complexes formation measured by fluorescence titration. Experimental data (symbols) and fitting curves (continuous lines) obtained at different wavelength as indicated in the legend with the assumption of A) 1:1 and B)1:1 and 1:2 protein-metal complexes formation. The parameters (log K1/K2 and Kd) calculated with Reactlab are indicated for each scenario.

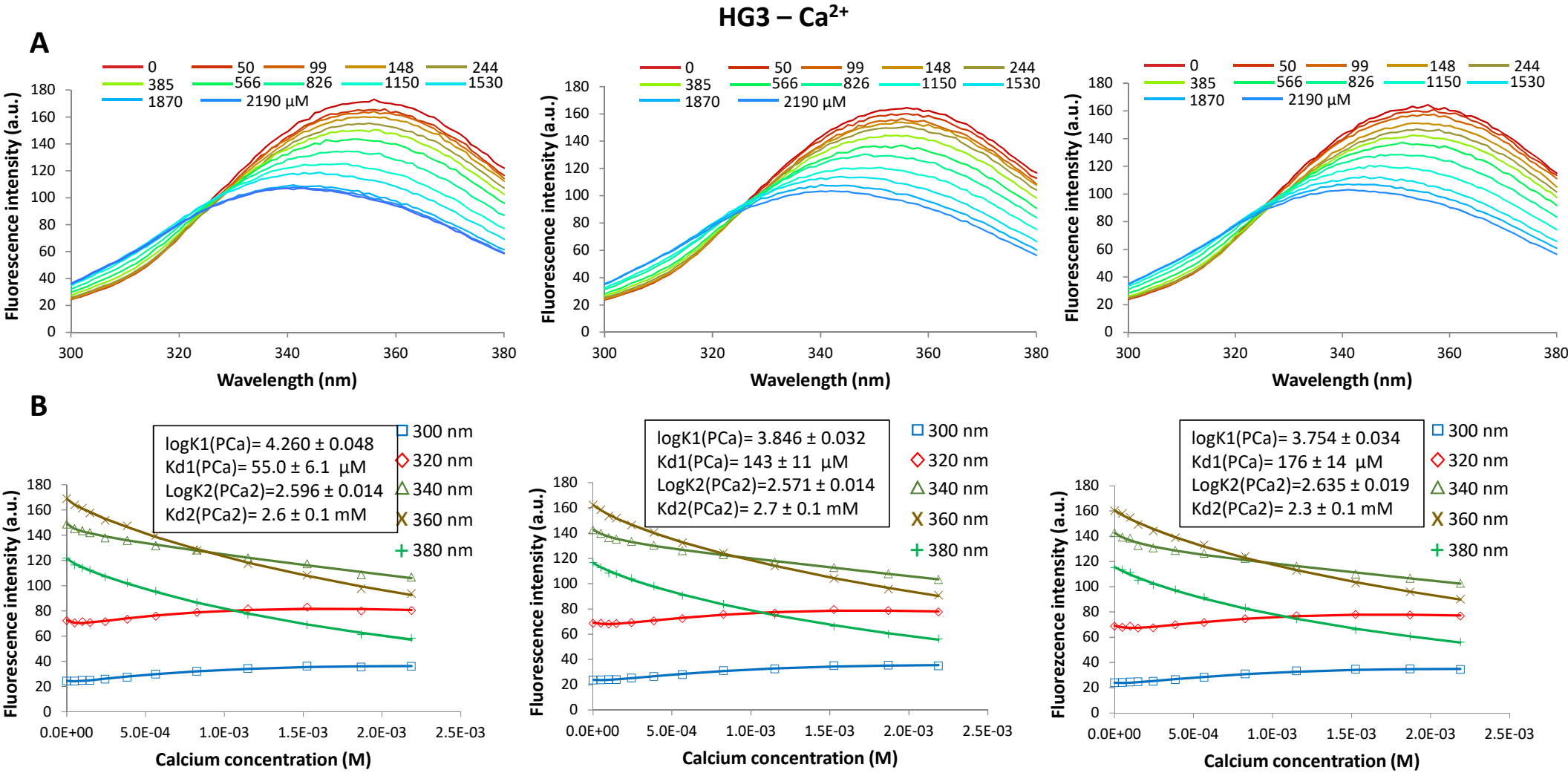

Fig. S22: Fluorescence spectra and fitting curves obtained with $UipA_{ext}$-HG3 protein and Ca^{2+} in a triplicate experiment. A) Fluorescence spectra recorded between 300 and 380 nm with different calcium concentrations (given in µM in the legend). B) Experimental data (symbols) and fitting curves (continuous lines) obtained at different wavelength as indicated in the legend with the assumption of 1:1 and 1:2 protein metal complexes formation. For each replicate, logK1(1:1 protein metal complex), logK2(1:2 protein metal complex) and the dissociation constant ($Kd=1/10^{logK}$) calculated in Reactlab are indicated.

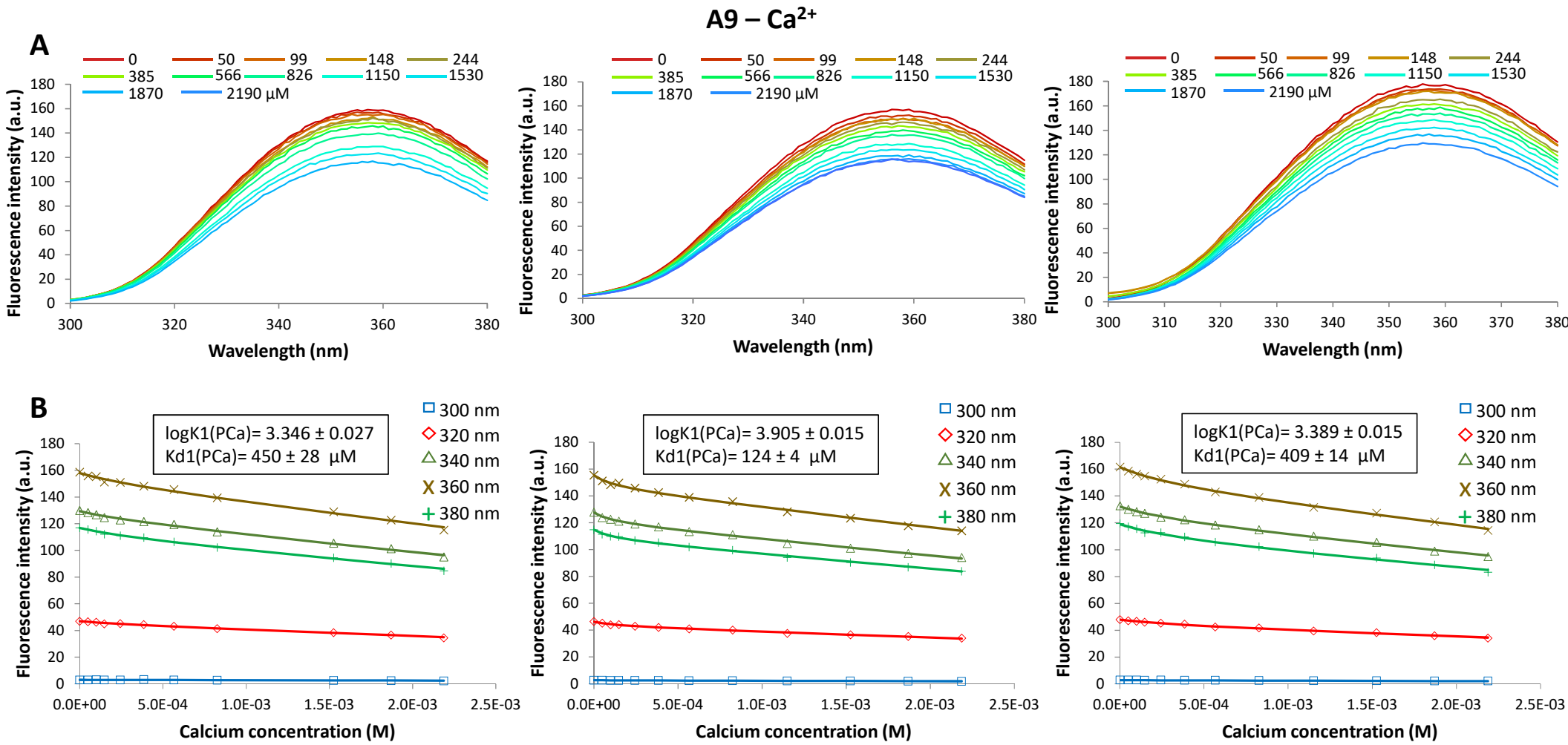

Fig. S23: Fluorescence spectra and fitting curves obtained with $UipA_{ext}$-A9 protein and Ca^{2+} in a triplicate experiment. A) Fluorescence spectra recorded between 300 and 380 nm with different calcium concentrations (given in µM in the legend). B) Experimental data (symbols) and fitting curves (continuous lines) obtained at different wavelength as indicated in the legend with the assumption of 1:1 protein metal complexes formation. For each replicate, logK1(PCa complex) and the dissociation constant $Kd1(PCa)=1/10^{logK1(PCa)}$ calculated in Reactlab are indicated.

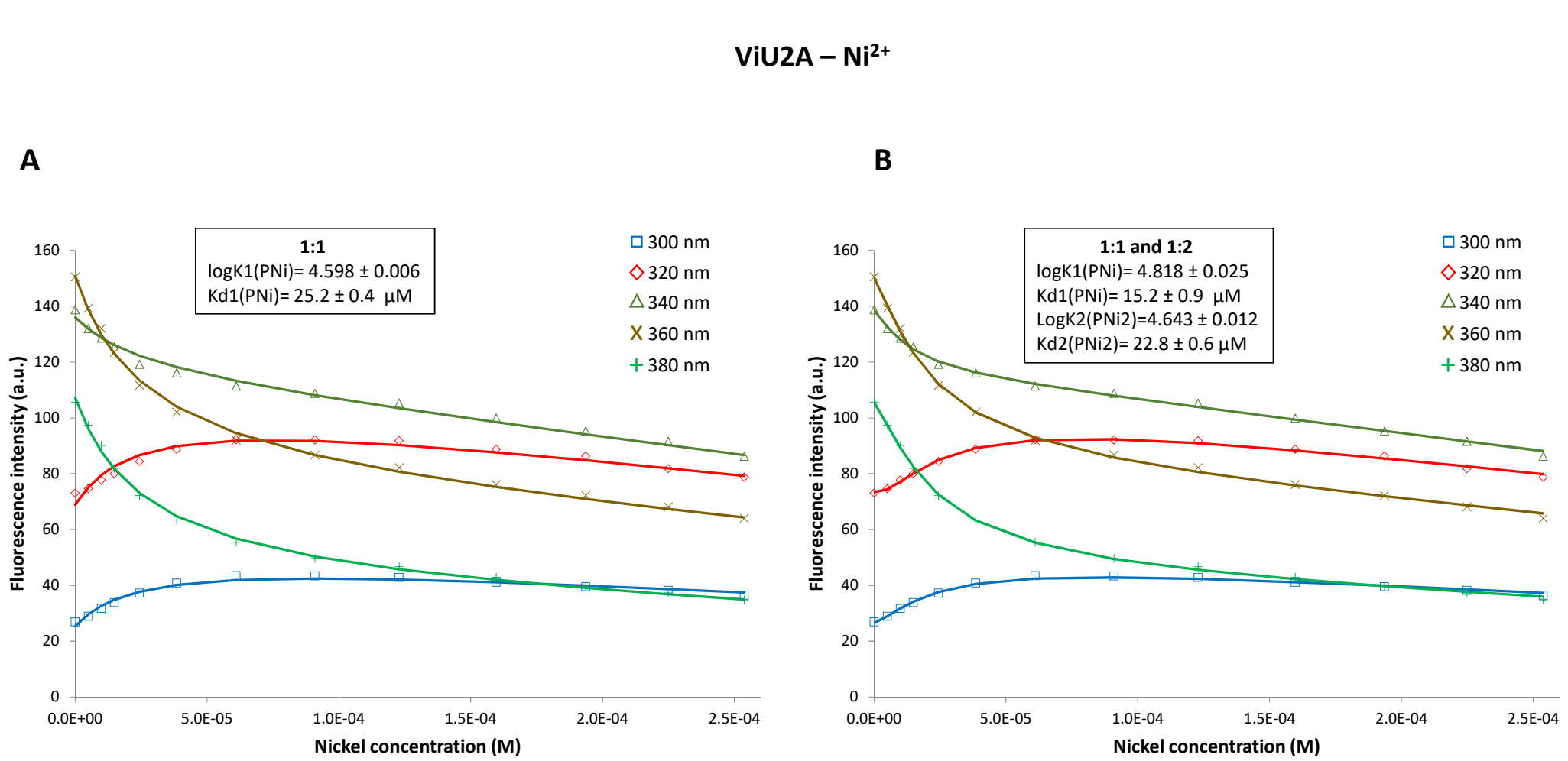

Fig. S24: Fitting curves for $UipA_{ext}$-ViU2A protein and Ni^{2+} complexes formation measured by fluorescence titration. Experimental data (symbols) and fitting curves (continuous lines) obtained at different wavelength as indicated in the legend with the assumption of A) 1:1 and B)1:1 and 1:2 protein-metal complexes formation. The parameters (log K1/K2 and Kd) calculated with Reactlab are indicated for each scenario.

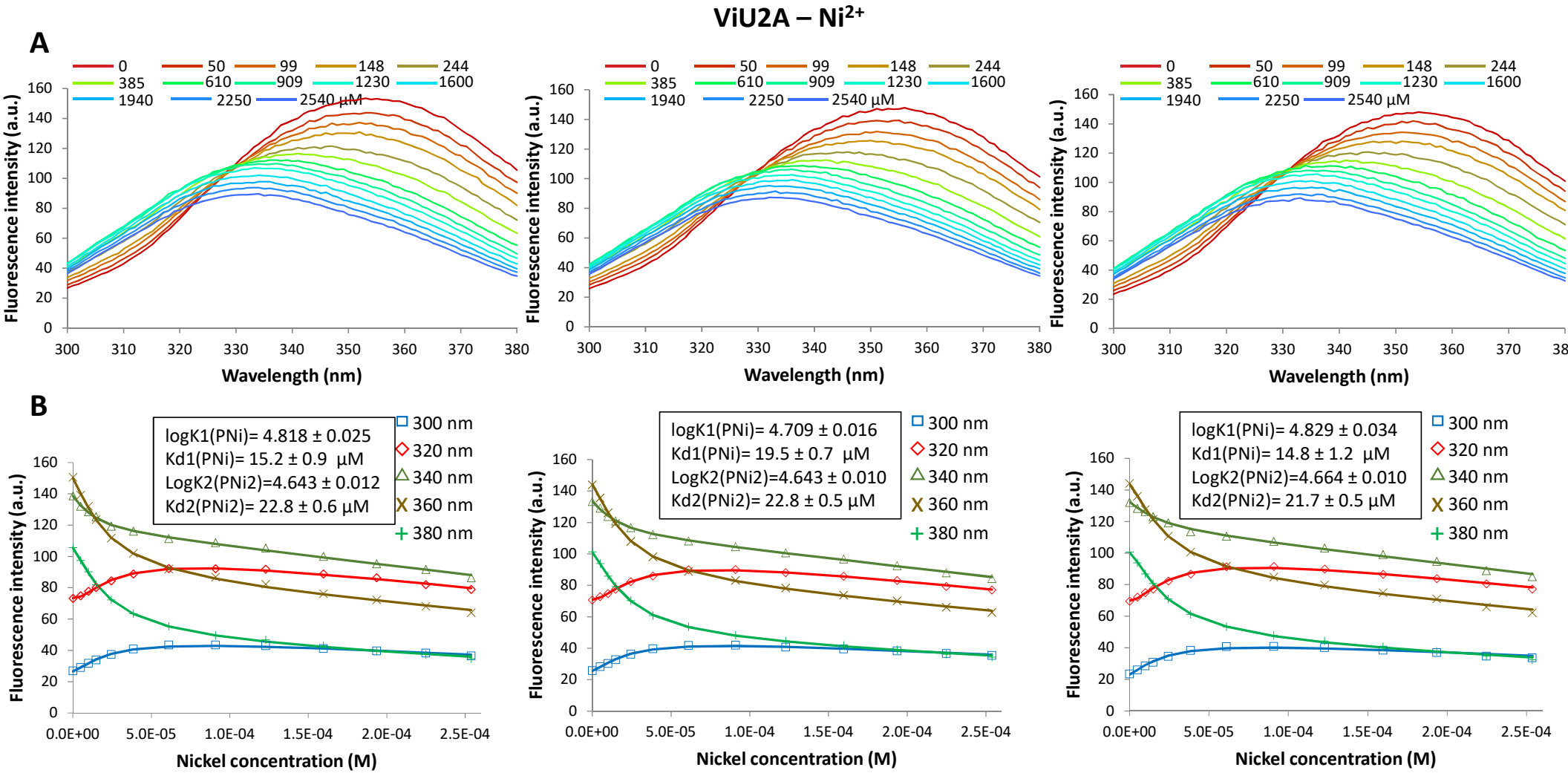

Fig. S25: Fluorescence spectra and fitting curves obtained with $UipA_{ViU2A}$-ext protein and Ni^{2+} in a triplicate experiment . A) Fluorescence spectra recorded between 300 and 380 nm with different nickel concentrations (given in µM in the legend). B) Experimental data (symbols) and fitting curves (continuous lines) obtained at different wavelength as indicated in the legend with the assumption of 1:1 and 1:2 protein metal complexes formation. For each replicate, logK1(1:1 protein metal complex), logK2(1:2 protein metal complex) and the dissociation constant ($Kd=1/10^{logK}$) calculated in Reactlab are indicated.

HG3 – Ni^{2+}

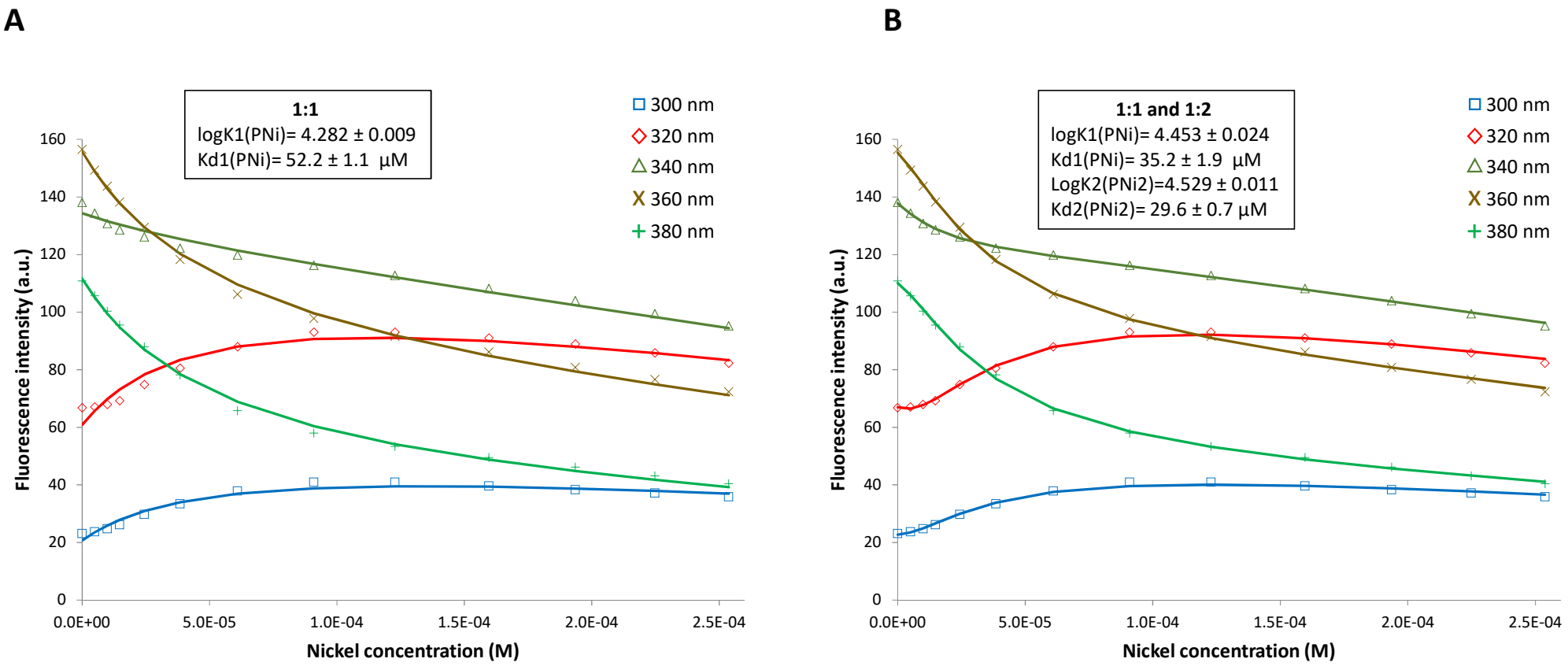

Fig. S26: Fitting curves for $UipA_{ext}$-HG3 protein and Ni^{2+} complexes formation measured by fluorescence titration. Experimental data (symbols) and fitting curves (continuous lines) obtained at different wavelength as indicated in the legend with the assumption of A) 1:1 and B)1:1 and 1:2 protein-metal complexes formation. The parameters (log K1/K2 and Kd) calculated with Reactlab are indicated for each scenario.

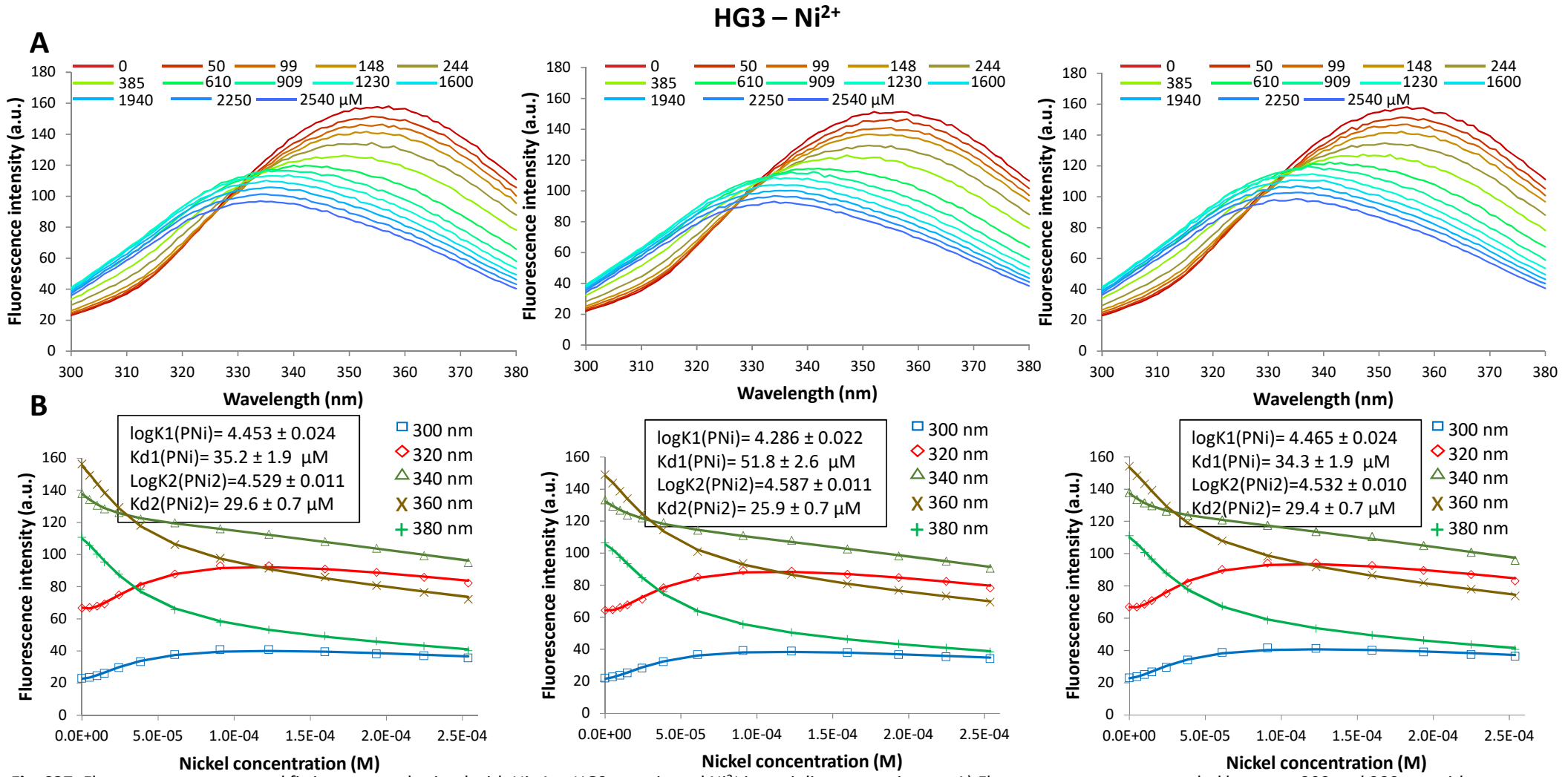

Fig. S27: Fluorescence spectra and fitting curves obtained with $UipA_{ext}$-HG3 protein and Ni^{2+} in a triplicate experiment. A) Fluorescence spectra recorded between 300 and 380 nm with different nickel concentrations (given in µM in the legend). B) Experimental data (symbols) and fitting curves (continuous lines) obtained at different wavelength as indicated in the legend with the assumption of 1:1 and 1:2 protein metal complexes formation. For each replicate, logK1(1:1 protein metal complex), logK2(1:2 protein metal complex) and the dissociation constant ($Kd=1/10^{logK}$) calculated in Reactlab are indicated.

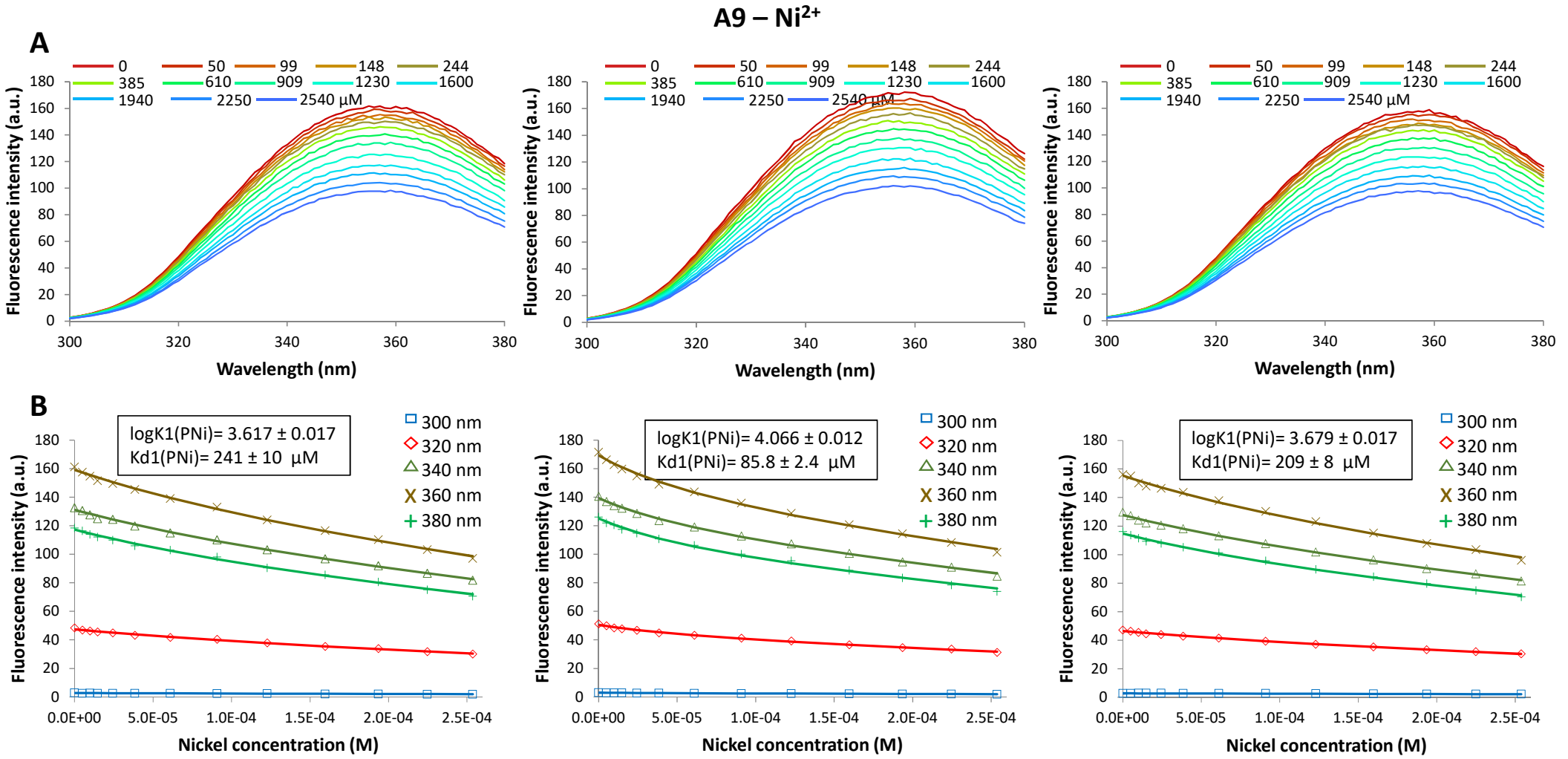

Fig. S28: Fluorescence spectra and fitting curves obtained with $UipA_{ext}$-A9 protein and Ni^{2+} in a triplicate experiment. A) Fluorescence spectra recorded between 300 and 380 nm with different nickel concentrations (given in µM in the legend). B) Experimental data (symbols) and fitting curves (continuous lines) obtained at different wavelength as indicated in the legend with the assumption of 1:1 protein metal complexes formation. For each replicate, logK1(PNi complex) and the dissociation constant $Kd1(PNi)=1/10^{logK1(PNi)}$ calculated in Reactlab are indicated.

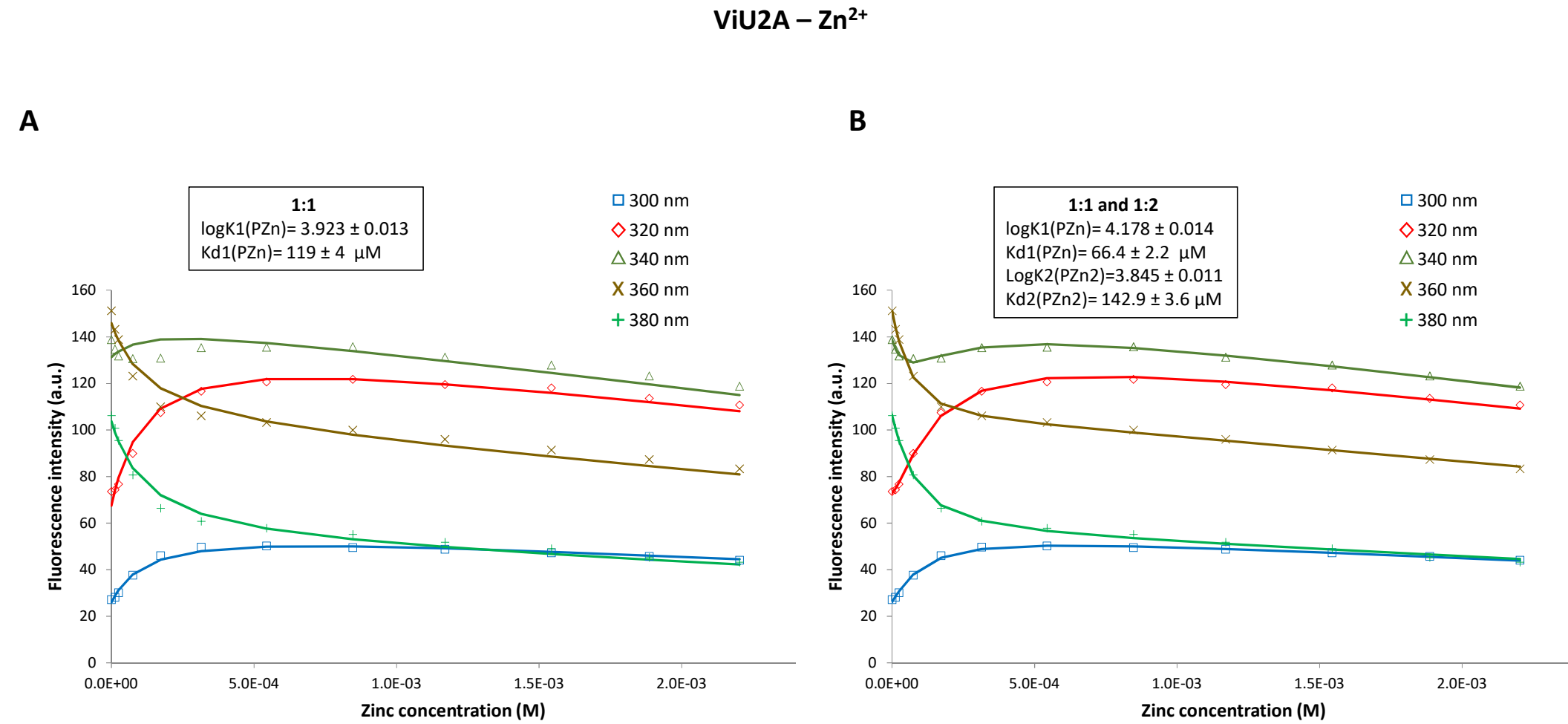

Fig. S29: Fitting curves for $UipA_{ext}$-ViU2A protein and Zn^{2+} complexes formation measured by fluorescence titration. Experimental data (symbols) and fitting curves (continuous lines) obtained at different wavelength as indicated in the legend with the assumption of A) 1:1 and B)1:1 and 1:2 protein-metal complexes formation. The parameters (log K1/K2 and Kd) calculated with Reactlab are indicated for each scenario.

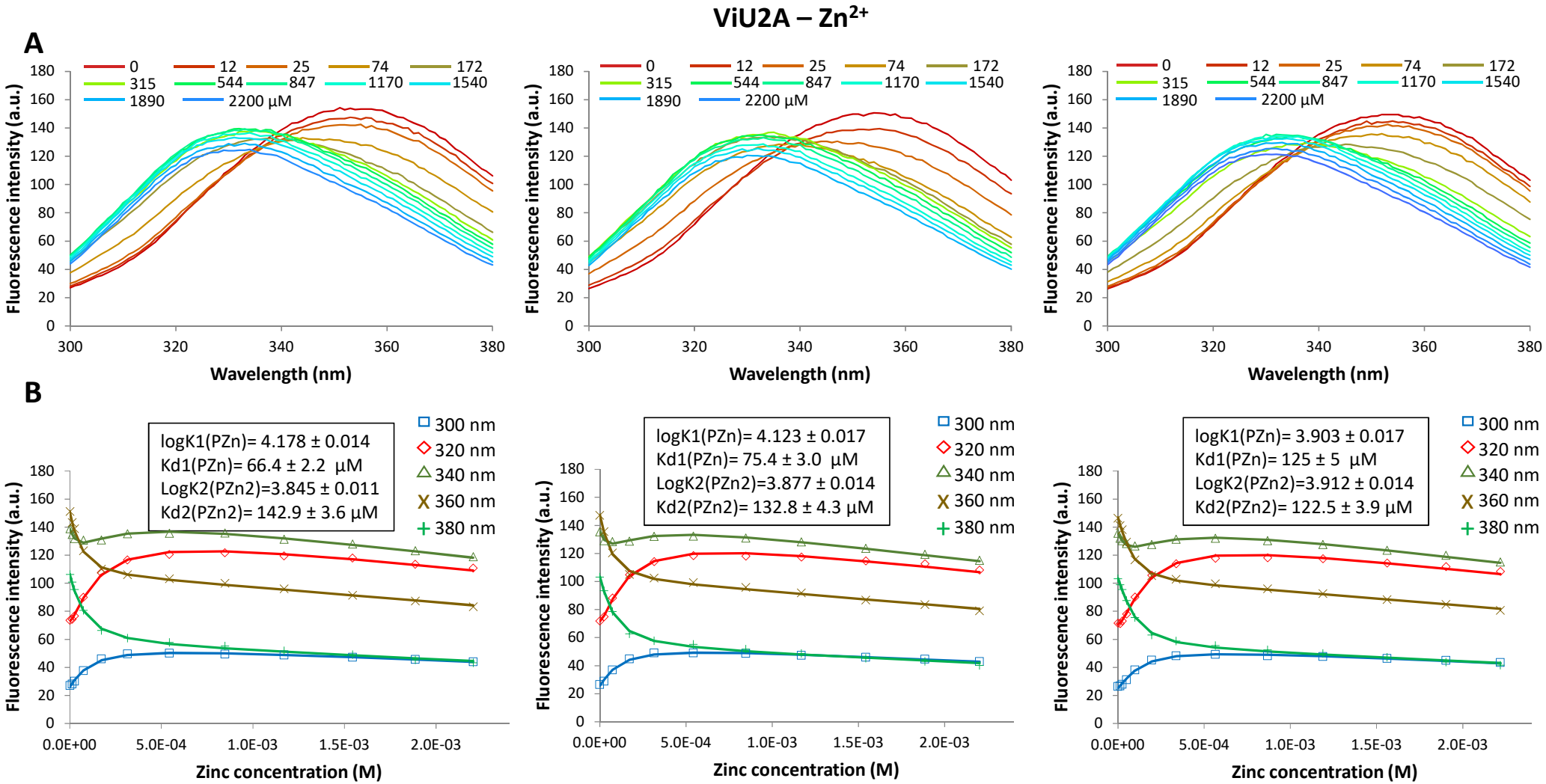

Fig. S30: Fluorescence spectra and fitting curves obtained with $UipA_{ViU2A}$-ext protein and Zn^{2+} in a triplicate experiment. A) Fluorescence spectra recorded between 300 and 380 nm with different zinc concentrations (given in µM in the legend). B) Experimental data (symbols) and fitting curves (continuous lines) obtained at different wavelength as indicated in the legend with the assumption of 1:1 and 1:2 protein metal complexes formation. For each replicate, logK1(1:1 protein metal complex), logK2(1:2 protein metal complex) and the dissociation constant ($Kd=1/10^{logK}$) calculated in Reactlab are indicated.

HG3 – Zn^{2+}

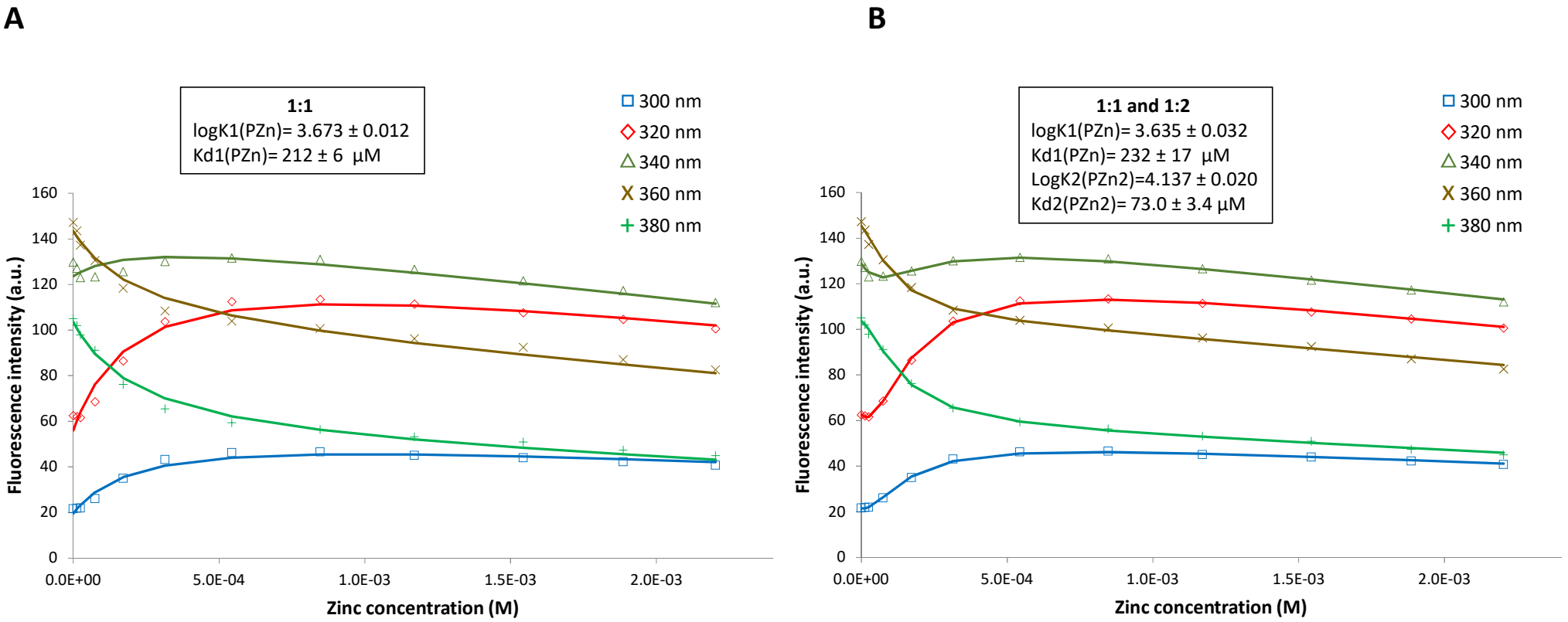

Fig. S31: Fitting curves for $UipA_{ext}$-HG3 protein and Zn^{2+} complexes formation measured by fluorescence titration. Experimental data (symbols) and fitting curves (continuous lines) obtained at different wavelength as indicated in the legend with the assumption of A) 1:1 and B)1:1 and 1:2 protein-metal complexes formation. The parameters (log K1/K2 and Kd) calculated with Reactlab are indicated for each scenario.

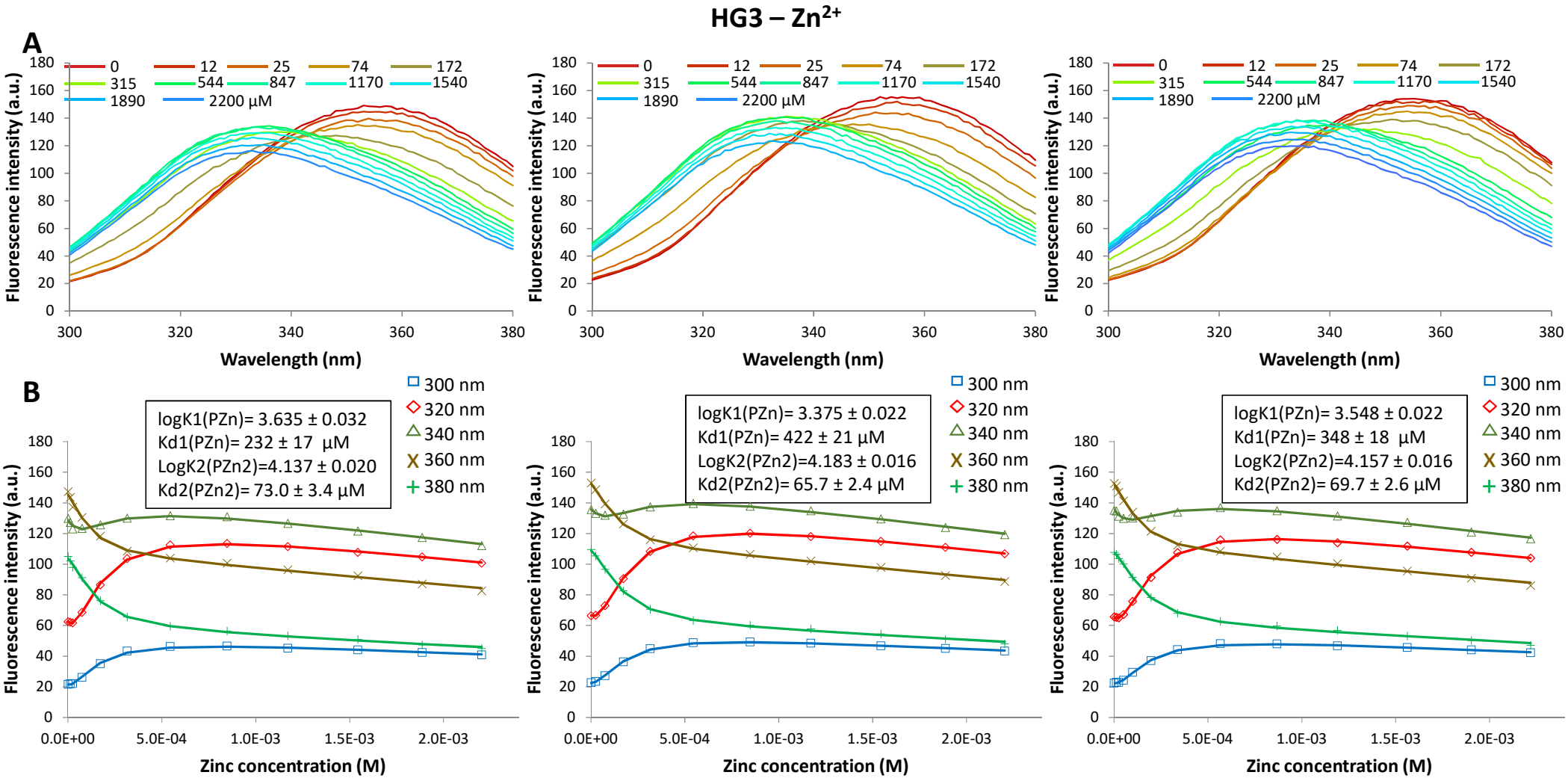

Fig. S32: Fluorescence spectra and fitting curves obtained with $UipA_{ext}$-HG3 protein and Zn^{2+} in a triplicate experiment. A) Fluorescence spectra recorded between 300 and 380 nm with different zinc concentrations (given in µM in the legend). B) Experimental data (symbols) and fitting curves (continuous lines) obtained at different wavelength as indicated in the legend with the assumption of 1:1 and 1:2 protein metal complexes formation. For each replicate, logK1(1:1 protein metal complex), logK2(1:2 protein metal complex) and the dissociation constant ($Kd=1/10^{logK}$) calculated in Reactlab are indicated.

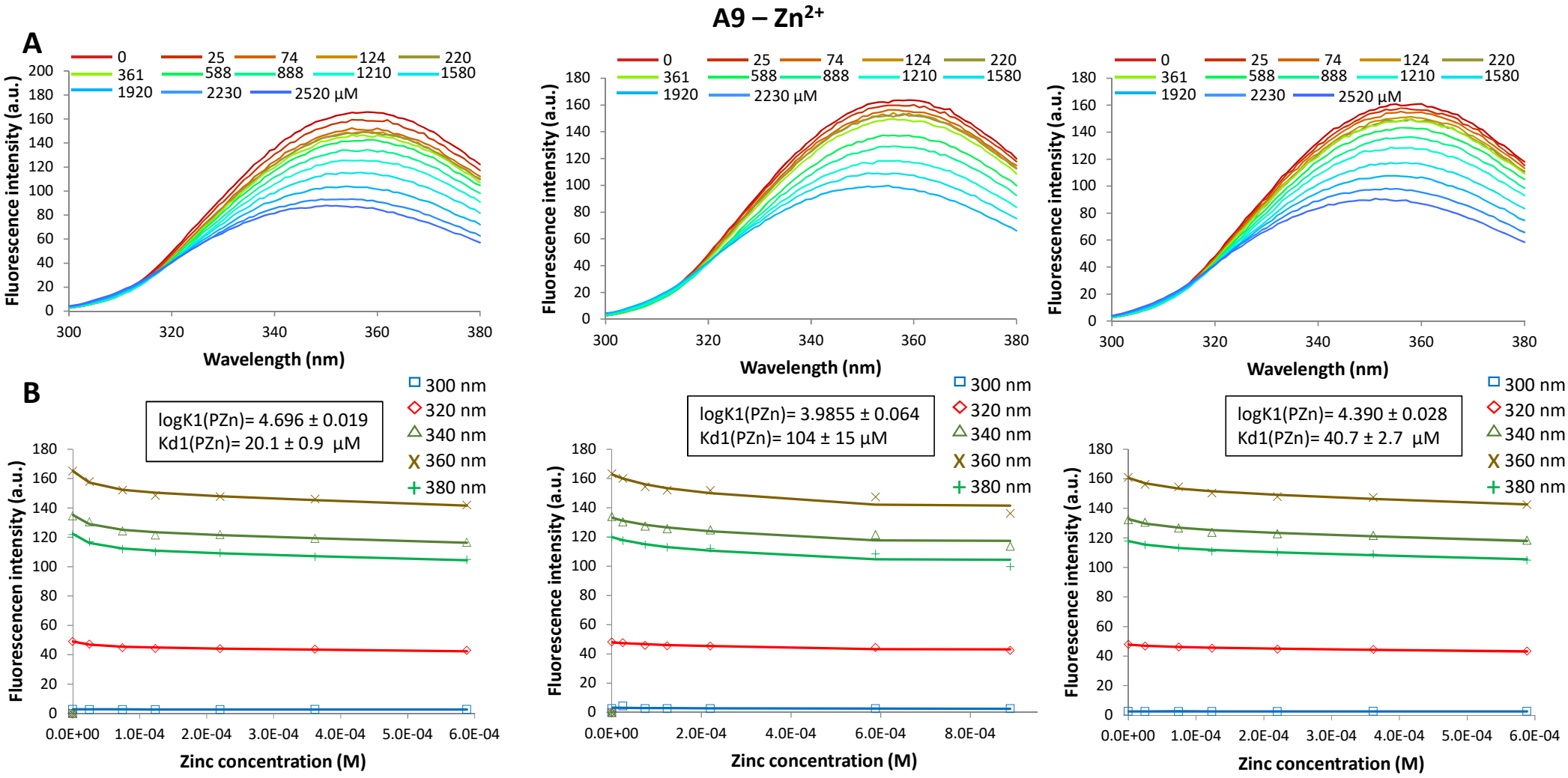

Fig. S33: Fluorescence spectra and fitting curves obtained with $UipA_{ext}$-A9 protein and Zn^{2+} in a triplicate experiment. A) Fluorescence spectra recorded between 300 and 380 nm with different zinc concentrations (given in µM in the legend). B) Experimental data (symbols) and fitting curves (continuous lines) obtained at different wavelength as indicated in the legend with the assumption of 1:1 protein metal complexes formation. For each replicate, logK1(PZn complex) and the dissociation constant $Kd1(PZn)=1/10^{logK1(PZn)}$ calculated in Reactlab are indicated.

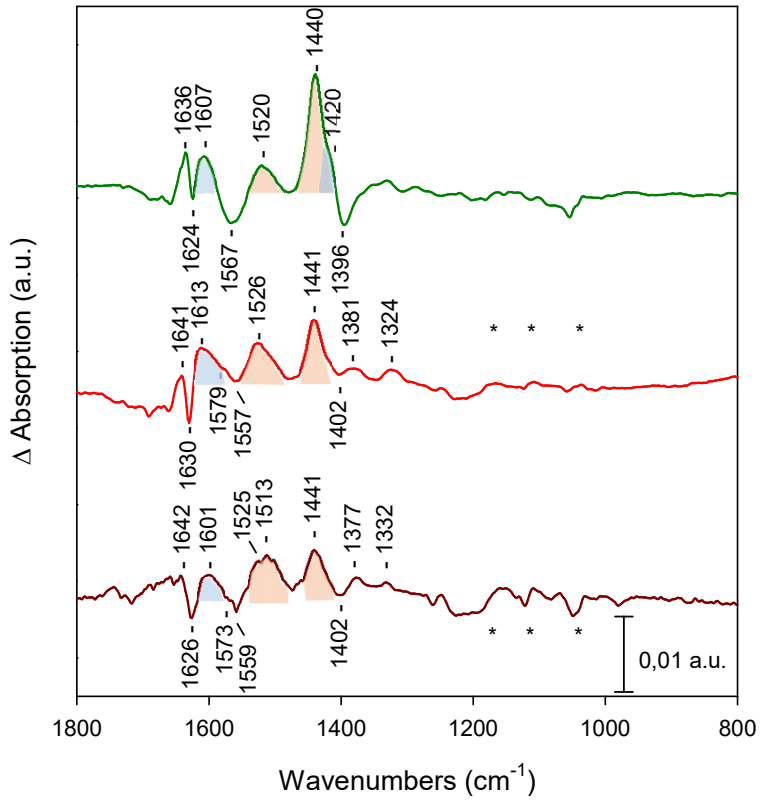

Fig. S34. FTIR difference spectra recorded with UipA-ext with Fe^{3+} – *minus* – without Fe^{3+}. Green line: $UipA_{ext}A9$, red line: $UipA_{ext}HG3$; brown line: $UipA_{ext}ViU2A$. * corresponds to IR bands of the MES Buffer.

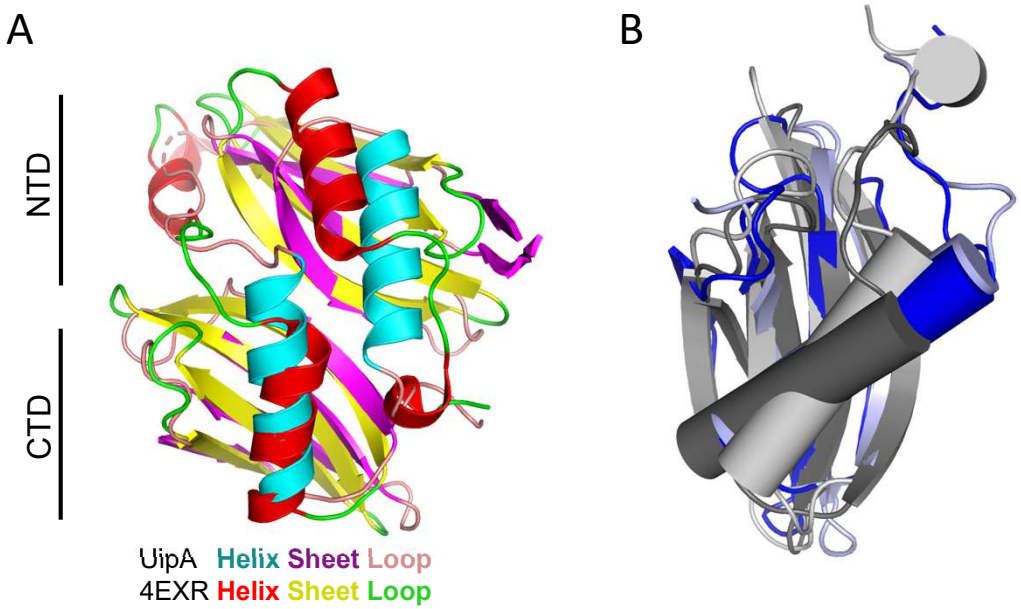

Fig. S35. Structural comparison between UipA and a putative lipoprotein (CD1622) from Clostridium difficile. A) Superimposition of the UipA pseudo-monomer with a putative lipoprotein (CD1622) from *Clostridium difficile* (pdb code 4EXR; unpublished). The overall topology is identical and, although the CTDs superimpose well, the main differences are in the NTD, which adopt a different orientation in both structures. B) Superimposition of the two domain of UipA (NTD and CTD in light-blue and dark-blue, respectively) with the two domains of the lipoprotein from *Clostridium difficile* (in light grey and dark-grey, respectively) showing that each domains adopt the same fold.

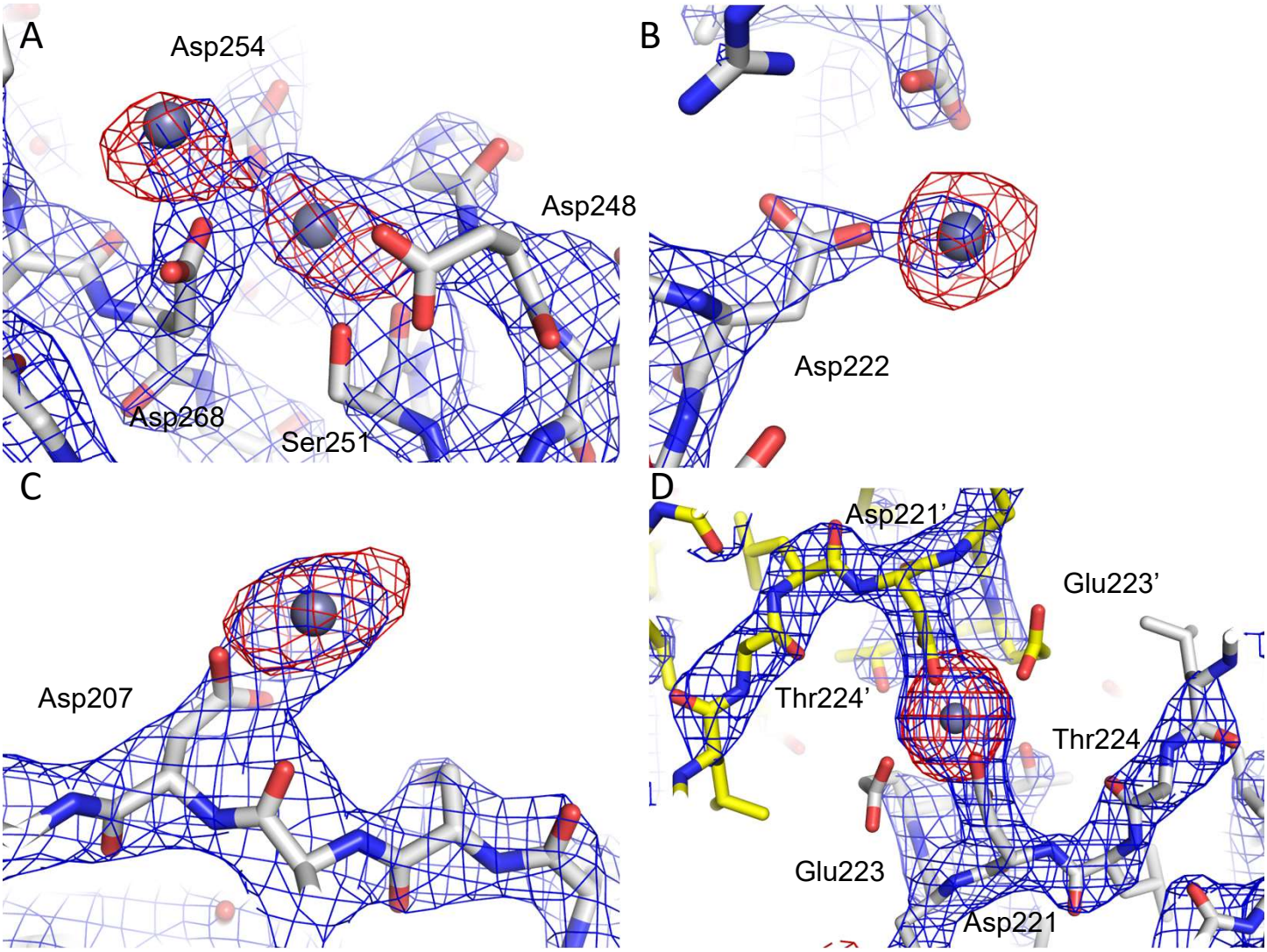

Fig. S36. Position of zinc sites in the crystal structure of $UipA_{ViU2A}$-out. (A, B, C, D) Details of five zinc stabilized in the structure of $UipA_{ViU2A}$-out, with the final refined $2F_{obs}$-F_{calc} map (blue) contoured at 2σ and the zinc anomalous map (red) contoured at 4σ. One zinc site (depicted in D) lies on the crystallographic two-fold axis, with the symmetry-related molecule depicted in yellow.

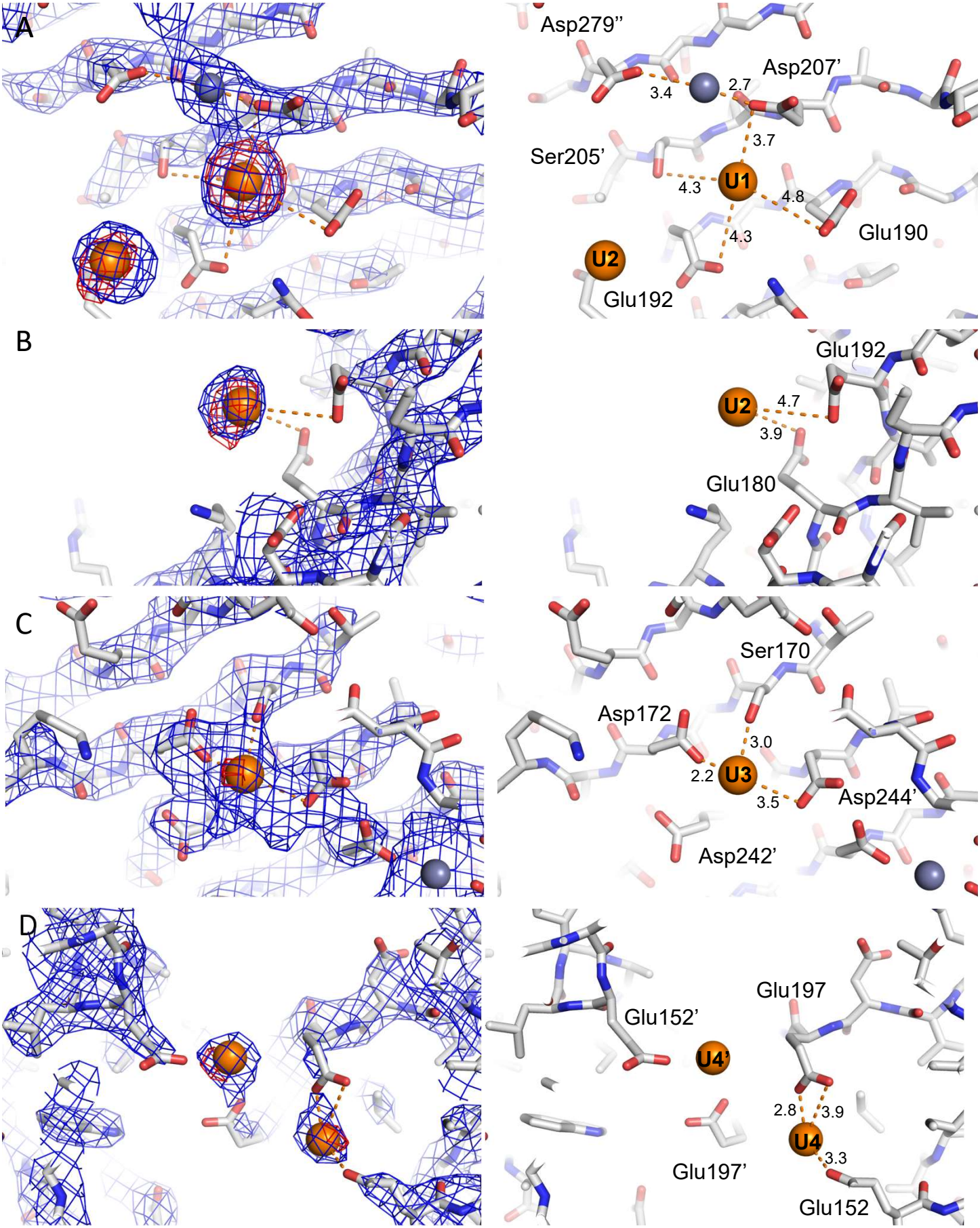

Fig. S37: Position of uranium sites in the crystal structure of $UipA_{ViU2A}$-out. (A-D) Details of the four uranium stabilized in the structure of $UipA_{ViU2A}$-out, with the final refined $2F_o$-F_c map (blue) contoured at 2σ and the uranium anomalous map (red) contoured at 4σ. Images on the right do not show the map for clarity and instead distance to uranium ions are indicated. The main uranium binding site is made of residues contributed by residues coming from both monomers of the domain-swapped dimer.

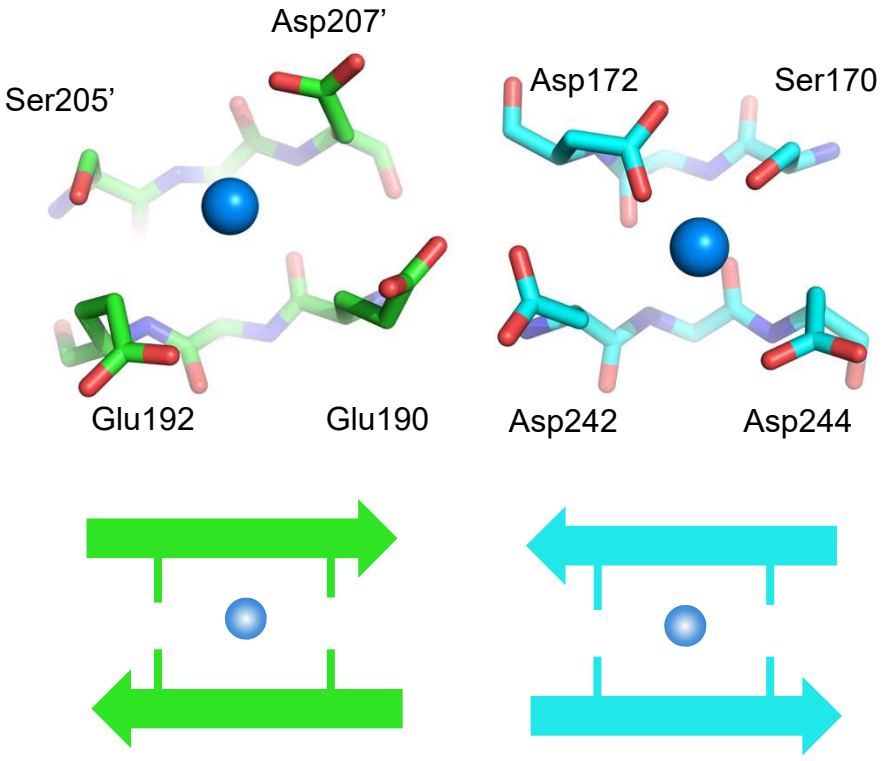

Fig. S38. Comparison of uranyl binding sites U1 and U3 (top: stick representation, bottom: scheme). Despite their resemblance (uranyl is pinched by four residues from two β-strands, with each chelating residues separated by one residue) both sites are not superimposable based solely on their secondary structure as β-strands are oriented in opposite directions.

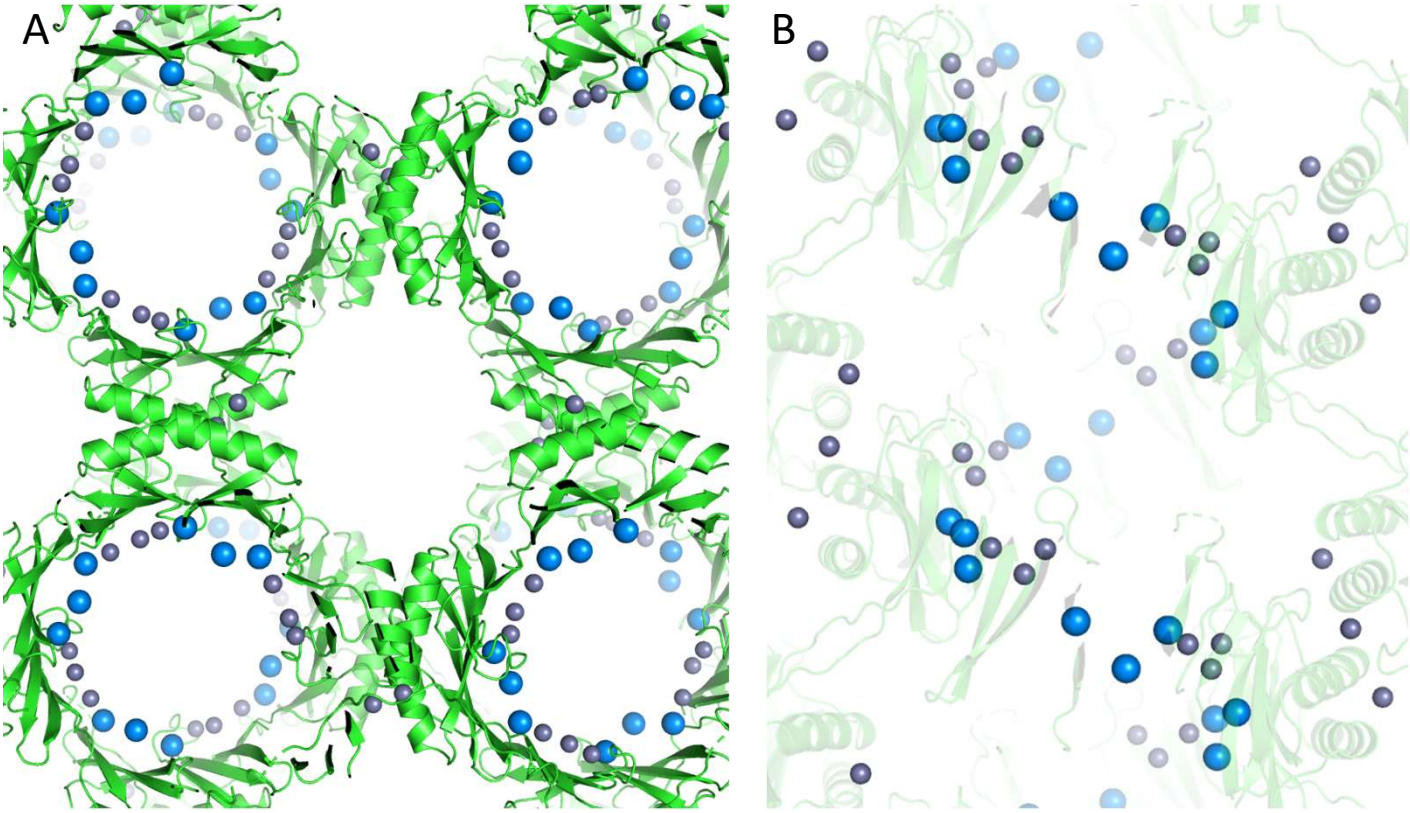

Fig. S39. Crystal packing of $UipA_{ViU2A}$-out and arrangement of metal binding site. (A) View along the 4_3 crystallographic axes, with UipA depicted as a cartoon, and uranium and zinc ions represented as spheres colored in blue and grey, respectively. Almost all the metals are projected along large solvent exposed channels. (B) View perpendicular to the 4_3 crystallographic axis, with transparent cartoons for clarity and along a single channel.

Table S5. Crystal data, data-collection and refinement statistics. Values in parentheses are for the highest

[#] $R_{merge} = \Sigma_{hkl} \Sigma_i |I_i(hkl) - (I(hkl))| / \Sigma_{hkl} \Sigma_i I_i(hkl)$, where $I_i(hkl)$ is the ith observation of reflection hkl and $\langle I(hkl) \rangle$ is the weighted average intensity for all observations of reflection hkl.

Data collection				
Data Set Name (pdb code)	**UipA-Native (7ATH)**		**UipA-Gd**	**UipA-U (7ATK)**
Wavelength	$\lambda_{high\ energy}$=0.99987	λ_{Zn}=1.28242	λ_{Gd}=1.71013	λ_{U}=1.3051
Space Group	$P\,4_12_12$	$P\,4_12_12$	$P\,4_12_12$	$P\,4_12_12$
Unit-cell parameters (Å)	a=b=96.1, c=52.6	a=b=96.1, c=52.6	a=b=95.3, c=53.2	a=b=95.2, c=52.5
Resolution range (Å)	43-2.2	48-2.4	47-2.6	47-2.9
High resolution range (Å)	2.3-2.2	2.6-2.4	2.8-2.6	3-2.9
Observed reflections	337 421 (53 761)	218 555 (39 878)	187 840 (22 023)	149 754 (23 451)
No. of unique reflections	23 892 (3 813)	17 562 (3 189)	14 337 (2 248)	10 684 (1 700)
Completeness (%)	99.8 (98.6)	100 (100)	99.6 (97.5)	99.6 (97.8)
CC1/2	99.9 (53.4)	99.8 (63.6)	99.6 (23.5)	99.9 (76.5)
$\langle I/\sigma(I) \rangle$	17.5 (1.0)	10.75 (1.1)	8.0 (0.7)	14.2 (1.9)
R_{merge}(%)[#]	7.0 (225.9)	12.5 (175.3)	0.8 (189.4)	13.6 (114.0)
Refinement				
Resolution range (Å)	43-2.3			47-2.9
R_{workt}/ R_{free}	21.8/24.7			20.7/23.4
No. of non-H atoms:				
Protein	962			962
Zn/U	5/-			05-avr
B-Factors				
Protein	39.6			88.5
ZN/U	115/-			111.9/173.9
R.m.s. deviation from ideal				
Bond lengths (Å)	0.011			0.008
Bond angles (°)	1.84			1.78

Table S8. Crystal data, data-collection and refinement statistics. Values in parentheses are for the highest

[#] $R_{merge} = \Sigma_{hkl} \Sigma_i |I_i(hkl) - (I(hkl))| / \Sigma_{hkl} \Sigma_i I_i(hkl)$, where $I_i(hkl)$ is the ith observation of reflection hkl and $\langle I(hkl) \rangle$ is the weighted average intensity for all observations of reflection hkl.

Data collection				
Data Set Name (pdb code)	**UipA-Native (7ATH)**		**UipA-Gd**	**UipA-U (7ATK)**
Wavelength	$\lambda_{high\ energy}$=0.99987	λ_{Zn}=1.28242	λ_{Gd}=1.71013	λ_{U}=1.3051
Space Group	$P\,4_12_12$	$P\,4_12_12$	$P\,4_12_12$	$P\,4_12_12$
Unit-cell parameters (Å)	a=b=96.1, c=52.6	a=b=96.1, c=52.6	a=b=95.3, c=53.2	a=b=95.2, c=52.5
Resolution range (Å)	43-2.2	48-2.4	47-2.6	47-2.9
High resolution range (Å)	2.3-2.2	2.6-2.4	2.8-2.6	3-2.9
Observed reflections	337 421 (53 761)	218 555 (39 878)	187 840 (22 023)	149 754 (23 451)
No. of unique reflections	23 892 (3 813)	17 562 (3 189)	14 337 (2 248)	10 684 (1 700)
Completeness (%)	99.8 (98.6)	100 (100)	99.6 (97.5)	99.6 (97.8)
CC1/2	99.9 (53.4)	99.8 (63.6)	99.6 (23.5)	99.9 (76.5)
$\langle I/\sigma(I) \rangle$	17.5 (1.0)	10.75 (1.1)	8.0 (0.7)	14.2 (1.9)
R_{merge}(%)[#]	7.0 (225.9)	12.5 (175.3)	0.8 (189.4)	13.6 (114.0)
Refinement				
Resolution range (Å)	43-2.3			47-2.9
R_{workt}/ R_{free}	21.8/24.7			20.7/23.4
No. of non-H atoms:				
Protein	962			962
Zn/U	5/-			05-avr
B-Factors				
Protein	39.6			88.5
ZN/U	115/-			111.9/173.9
R.m.s. deviation from ideal				
Bond lengths (Å)	0.011			0.008
Bond angles (°)	1.84			1.78